

Dark-Matter Halo Profiles of a General Cusp/Core with Analytic Velocity and Potential

Avishai Dekel¹, Guy Ishai¹, Aaron A. Dutton², Andrea V. Macciò^{2,3}

¹*Racah Institute of Physics, The Hebrew University, Jerusalem 91904 Israel*

²*New York University Abu Dhabi, PO Box 129188, Abu Dhabi, United Arab Emirates*

³*Max-Planck-Institut für Astronomie, Königstuhl 17, 69117 Heidelberg, Germany*
 dekel@huji.ac.il

14 March 2017

ABSTRACT

We present useful functions for the profiles of dark-matter (DM) haloes with a free inner slope, from cusps to cores, where the profiles of density, mass-velocity and *potential* are simple analytic expressions. Analytic velocity is obtained by expressing the mean density as a simple functional form, and deriving the local density by differentiation. The function involves four shape parameters, with only two or three free: a concentration parameter c , inner and outer asymptotic slopes α and $\bar{\gamma}$, and a middle shape parameter β . Analytic expressions for the potential and velocity dispersion exist for $\bar{\gamma} = 3$ and for β a natural number.

We match the models to the DM haloes in cosmological simulations, with and without baryons, ranging from steep cusps to flat cores. Excellent fits are obtained with three free parameters (c , α , $\bar{\gamma}$) and $\beta = 2$. For an analytic potential, similar fits are obtained for $\bar{\gamma} = 3$ and $\beta = 2$ with only two free parameters (c , α); this is our favorite model. A linear combination of two such profiles, with an additional free concentration parameter, provides excellent fits also for $\beta = 1$, where the expressions are simpler. The fit quality is comparable to non-analytic popular models.

An analytic potential is useful for modeling the inner-halo evolution due to gas inflows and outflows, studying environmental effects on the outer halo, and generating halo potentials or initial conditions for simulations. The analytic velocity can quantify simulated and observed rotation curves without numerical integrations.

Key words: dark matter — galaxies: evolution — galaxies: formation — galaxies: structure — galaxies: haloes

1 INTRODUCTION

The shapes of the density profiles of dark-matter haloes, as deduced from cosmological N-body simulations of DM only (DMO), are commonly fit by a function with one free parameter, such as the NFW profile (Navarro, Frenk & White 1997). This profile has a fixed power-law cusp at small radii with an asymptotic log slope $-\alpha$ where $\alpha = 1$, and a fixed asymptotic slope $-\gamma$ with $\gamma = 3$ at large radii. The free parameter is the characteristic radius r_c of the inner cusp/core, which can be replaced by the concentration parameter c , defined by $c = R_v/r_c$, where R_v is the halo virial radius, determined by the halo mass and cosmological time. However, simulated halo profiles, especially when baryons are included, may show deviations from this universal shape both in the inner cusp and in the outskirts near the halo virial radius R_v , as well as in between.

In particular, the observed halo profiles, especially in low-mass galaxies, tend to have a flatter cusp, with $\alpha < 1$, and possibly even a constant-density core, $\alpha \simeq 0$ (de Blok et al. 2001; Swaters et al. 2003; Goerdt et al. 2006; Walker & Peñarrubia 2011; Oh et al. 2011), while massive galaxies may show a steeper cusp, $\alpha > 1$. Within the standard cosmology with non-interacting cold dark matter, the common wisdom is that the baryonic processes associated with galaxy formation and evolution are responsible for strong evolution of the DM inner profiles, steepening the cusp in massive haloes and flattening it in lower-mass haloes, potentially all the way to a flat core with $\alpha = 0$ (e.g., simulations by Tollet et al. 2016, and references therein). On the other side, environmental tidal effects may alter the halo profile in the outskirts (e.g. More, Diemer & Kravtsov 2015). For the modeling of the halo profile as it evolves

between cusp and core, or as it is stripped from the outside, and for quantifying the variety of simulated and observed velocity profiles, one desires to have a function with more freedom than the NFW profile. In addition to the free concentration parameter, a free inner slope α can help matching the variations between a cusp and a core, a free outer slope γ may provide a flexibility at the outskirts when necessary, and an intermediate shape parameter β may improve the fit in the middle halo when very high accuracy is desired.

While the profile has to provide a good fit to the variety of DM-halo profiles with a minimum number of free parameters, our desire is to have *analytic* expressions both for the density profile and for the integrated mass profile, which immediately translates to the DM circular velocity profile that can be deduced from observations. Furthermore, we wish to have an analytic expression for the gravitational potential profile, being crucial, e.g., for the analytic modeling of the evolution between a cusp and a core. In addition, an analytic expression for the velocity-dispersion profile may help constructing DM haloes in equilibrium, e.g., as initial conditions for simulations.

Several density profiles with different levels of flexibility in the inner slope have been proposed and some are widely used (Einasto 1965; Jaffe 1983; Hernquist 1990; Dehnen 1993; Tremaine et al. 1994; Evans 1994; Burkert 1995; Zhao 1996; Jing & Suto 2000; Navarro et al. 2004; Stoehr 2006; Merritt et al. 2006; Di Cintio et al. 2014; Schaller et al. 2015; Oldham & Auger 2016). In particular, the Einasto profile (Einasto 1965; Navarro et al. 2004, see eq. (37)), with one additional free shape parameter, provides an excellent fit to the cusps of DM-only simulated haloes. Unfortunately, it does not have sufficient flexibility to accommodate inner cores (§4.3). Among the profiles with a flexible inner slope, the profile proposed by Dehnen (1993) and Tremaine et al. (1994) stands out as having analytic expressions for the density, mass and potential. It is useful in modeling spherical stellar systems, but as is, with only one free shape parameter, it does not have the flexibility for a good fit to DM haloes. This analytic profile can be partly generalized with an additional parameter β that characterizes the transition region between the asymptotic regions (Zhao 1996), but this by itself still does not provide the flexibility required for fitting DM haloes. To the best of our knowledge, the profiles used so far that can resemble the variety of DM haloes do not have analytic expressions for the mass-velocity or potential profiles. Analytic expressions are limited to special cases, such as the NFW cusp with $\alpha = 1$, or a similar profile with $\alpha = 0$, as well as other special cases (summarized in Zhao 1996). The desired analytic expressions are missing for profiles that fit DM haloes with sufficient flexibility in the inner and outer regions.

Here we propose profiles of the desired analytic nature, which fit very well the profiles of DM haloes with a general cusp-core. The first has simple analytic expressions for the density and mass-velocity profiles in the general case of a free outer slope. The two others also

have analytic potentials for a general inner slope α with the outer asymptotic slope of the local density $\rho(r)$ fixed at either $\gamma = 4$ or $\gamma = 3.5$, both corresponding to a slope $\bar{\gamma} = 3$ for the mean-density profile $\bar{\rho}(r)$. The asymptotic outer slope, which is materialized well outside the halo virial radius, is compensated for by a proper choice of another parameter, the concentration parameter c . The case $\gamma = 3.5$, with a proper choice of middle shape parameter $\beta = 2$ (see below), provides excellent fits to simulated haloes with only two free parameters. The case $\gamma = 4$ provides adequate fits, which become excellent once a sum of two such functions is considered, with an additional free concentration parameter. Our proposed profiles are inspired by earlier ideas concerning analytic integrals (e.g. Dehnen 1993; Tremaine et al. 1994; Zhao 1996), combined with a concentration parameter (e.g. Navarro, Frenk & White 1997), and if necessary a linear combination of two functions (e.g. Zhao 1996; Schaller et al. 2015).

In §2 we present the flexible profile with analytic density and mass-velocity. In §3 we present the profiles with fixed outer slopes that also provide analytic expressions for the potential and velocity dispersion profiles, with either two or three free parameters. In §4 we compare the fits of the different proposed model profiles to simulated halo profiles with and without baryons, spanning a variety of cusps and cores. We then compare the new analytic models to other fitting functions that do not have analytic expressions for mass-velocity and potential. In §5 we summarize and discuss our results.

2 A FLEXIBLE PROFILE WITH ANALYTIC MASS-VELOCITY AND DENSITY

2.1 Introduction: A General Non-analytic Profile

As an introductory reference, consider the very flexible and commonly used functional form for the shape of the density profile (sometimes termed the $\alpha\beta\gamma^1$ profile),

$$\rho(r) = \frac{\rho_c}{x^\alpha(1+x^{1/\beta})^{\beta(\gamma-\alpha)}}, \quad (1)$$

where we scale the radius by an intermediate radius r_c , related to R_v by a concentration parameter c ,

$$x = \frac{r}{r_c}, \quad r_c = \frac{R_v}{c}. \quad (2)$$

The DM-halo virial radius R_v is the physical scale determined by cosmology at a given time for a given halo mass, so for the sake of studying halo profile shapes we measure distances r with respect R_v , and replace r_c by c as a free parameter. The parameters α and γ are the asymptotic slopes of $\log \rho(r)$ at $x \ll 1$ and $x \gg 1$ respectively. The parameter β characterizes the shape near the transition radius $x \sim 1$. The characteristic density ρ_c can be expressed in terms of $\bar{\rho}_v$, the mean mass density within R_v , defined to be, e.g., a factor of 200 larger than the cosmological critical mean density. This

¹ Note that different authors may use different permutations of these parameters.

functional form thus has in principle four shape parameters, α , β , γ and c . We will see in §4 that for the purpose of fitting DM haloes from simulations with analytic expressions one can do with three and even only two free parameters. As will be discussed in §2.2.5, the parameters in eq. (1) do not necessarily have a straightforward physical meaning, but they can be replaced by more physical parameters.

The general functional form of eq. (1) reduces to the standard NFW profile (Navarro, Frenk & White 1997) for $\alpha = 1$, $\beta = 1$, and $\gamma = 3$, leaving c as the single free shape parameter. In this case the slope of $\rho(r)$ at r_c is -2 . The NFW profile has been extremely useful in fitting the density profiles of DM haloes in cosmological simulations of dark matter only (DMO) with no baryons. With one or more of the additional parameters free, eq. (1) may provide the flexibility required for fitting the profiles of haloes that have been modified by baryonic processes or environmental effects.

The associated profiles of mass and velocity are needed, e.g., for comparison with observed rotation curves. The associated profiles of potential and velocity dispersion are needed, e.g., for analytic modeling of halo evolution. In special cases, e.g., when α , β and γ are natural numbers, as in NFW, it may be possible to obtain analytic expressions for all these profiles. However, observed haloes, as well as haloes simulated with baryons or in clustered environments, require that the parameters, especially α , are general real numbers. In most such cases, one has to perform numerical integrations of eq. (1) in order to yield the mass-velocity, potential and velocity dispersion profiles. The same is true for most other functional forms that have been used to fit DM haloes. This includes in particular the Einasto profile (Einasto 1965; Navarro et al. 2004; Merritt et al. 2006; Graham et al. 2006; Gao et al. 2008; Dutton & Macciò 2014), which provides better fits than NFW to DMO-simulated profiles. It also includes other profiles that allow a match to simulated profiles which deviate from the NFW or the Einasto profiles (e.g. Di Cintio et al. 2014; Schaller et al. 2015).

In order to enable straightforward comparisons to observed rotation curves, and in order to quantify the effects of baryons on the inner halo and environment on the outer halo, we seek a functional form with free inner and outer slopes in which the profiles of density and mass-velocity are given by analytic expressions. For the purpose of an analytic study of the evolution of the inner halo due to baryonic processes, we require that the potential profile should also be analytic. An analytic isotropic velocity dispersion will enable constructing a DM halo in equilibrium. In the following subsection we propose a modification of the flexible multi-parameter profile of eq. (1) that allows analytic expressions for the mass and velocity profiles. Then in §3 we introduce special cases of this profile which also have analytic potential and velocity dispersion and are very useful in fitting the variety of DM halo profiles with only two or three free shape parameters.

2.2 Analytic Mass-Velocity and Density

2.2.1 Mean density

The idea for obtaining analytic density and mass-velocity profiles is very simple. We apply a functional form inspired by eq. (1), but to the *mean* density within the sphere of radius r (or equivalently to the mass or velocity profiles) rather than to the local density at r , namely

$$\bar{\rho}(r) = \frac{\bar{\rho}_c}{x^\alpha(1+x^{1/\beta})^{\beta(\bar{\gamma}-\alpha)}}, \quad x = \frac{r}{r_c}, \quad r_c = \frac{R_v}{c}. \quad (3)$$

The local density profile is then determined by a straightforward derivative. The mass, velocity and force profiles are derived straightforwardly from $\bar{\rho}(r)$. For certain specific choices of β and $\bar{\gamma}$, the potential profile is derived by analytic integration, for a general value of α (§3).

Now the parameters refer to $\bar{\rho}(r)$ rather than $\rho(r)$, and we explicitly distinguish the asymptotic outer slopes $\bar{\gamma}$ and γ in eq. (3) and eq. (1). The parameter c , as in eq. (1), refers to an inner radius, $r_c = R_v/c$, that marks the middle-halo transition between the asymptotic slopes of $\bar{\rho}(r)$, though the slope there, for either $\bar{\rho}$ or ρ , is in general not -2 (as it is for NFW), so its interpretation as a characteristic intermediate radius can be dubious. For the purpose of studying the profile shape, we measure the radius r in terms of the virial radius R_v , so that r_c in eq. (3) is replaced by c^{-1} .

The normalization factor $\bar{\rho}_c$ in eq. (3) is expressed as a function of $\bar{\rho}_v$ and the shape parameters,

$$\bar{\rho}_c = c^3 \mu \bar{\rho}_v, \quad (4)$$

where

$$\mu = \frac{(1+c^{1/\beta})^{\beta(\bar{\gamma}-\alpha)}}{c^{(3-\alpha)}}. \quad (5)$$

For the purpose of comparing profile shapes, we measure the density by means of $\bar{\rho}_v$, and the mass and velocity by means of the virial mass M_v and velocity V_v .² The shape of this very flexible profile can thus involve four parameters: α , β , $\bar{\gamma}$ and c .

If the profile has a power-law inner cusp or core, the same α represents the asymptotic inner slope of both $\bar{\rho}$ and ρ . In the outer asymptote, we first address here the profiles of density, mass and velocity for a general $\bar{\gamma}$, which are very flexible in matching the outskirts of haloes subject to environmental effects. Then in §3 we appeal to special cases of $\bar{\gamma} = 3$, which have in addition analytic potentials and still provide excellent fits to the variety of DM halo profiles with only two or three free parameters.

² Recall that at a given cosmological time, for a given $\Delta_v = 200$ defining the virial radius, there is a one-to-one correspondence between all the virial quantities.

2.2.2 Mass, Velocity and Force

The mass profile is easily deduced from eq. (3),

$$M(r) = \frac{4\pi}{3} \bar{\rho}(r) r^3 = \mu M_v x^3 \bar{\rho}(r) / \bar{\rho}_c. \quad (6)$$

The velocity profile, the common observable, immediately follows (adopting hereafter $G = 1$),

$$V^2(r) = \frac{M(r)}{r} = c\mu V_v^2 x^2 \bar{\rho}(r) / \bar{\rho}_c, \quad (7)$$

where $V_v^2 = M_v / R_v$. The force profile is

$$F(r) = -\frac{M(r)}{r^2} = c^2 \mu F_v x \bar{\rho}(r) / \bar{\rho}_c, \quad (8)$$

where $F_v = -M_v / R_v^2$. Note that the maximum velocity is obtained at

$$x_{\max} = \left(\frac{2 - \alpha}{\bar{\gamma} - 2} \right)^\beta, \quad (9)$$

which is also where the slope of $\bar{\rho}(r)$ is -2 , but generally not where the slope of the local $\rho(r)$ is -2 (see §2.2.4 below). For $\alpha + \gamma = 4$ the peak velocity and mean-density slope of -2 coincide at $x = 1$. The maximum value of the velocity, for $c \gg 1$, is $V_{\max}^2 \propto c^{\bar{\gamma}-2}$.

2.2.3 Local Density

The local density profile is obtained from the mass profile by derivative,

$$\rho(r) = \frac{1}{4\pi r^2} \frac{dM}{dr}, \quad (10)$$

namely,

$$\rho(r) = \frac{3 - \alpha}{3} \left(1 + \frac{3 - \bar{\gamma}}{3 - \alpha} x^{1/\beta} \right) \frac{1}{(1 + x^{1/\beta})} \bar{\rho}(r). \quad (11)$$

For a general $\bar{\gamma} \neq 3$ this does not resemble the functional form of eq. (1) as the term in big parentheses involves a sum of two different powers of x . In the asymptotic inner-halo limit, $x \ll 1$, we do have $\rho \propto x^{-\alpha}$, as in $\bar{\rho}(r)$, with

$$\rho \simeq \frac{\rho_c}{x^\alpha}, \quad \bar{\rho} \simeq \frac{\bar{\rho}_c}{x^\alpha}, \quad \rho_c \simeq \frac{3 - \alpha}{3} \bar{\rho}_c, \quad V^2 \simeq c\mu V_v^2 x^{2-\alpha}. \quad (12)$$

In the asymptotic outskirts, $x \gg 1$, once $\bar{\gamma} \neq 3$, we have $\rho(r) \propto \bar{\rho}(r)$, namely $\rho \propto x^{-\gamma}$ with $\gamma = \bar{\gamma}$. However, for $\bar{\gamma}$ near 3, this slope may be materialized only well beyond the virial radius.

For the special case $\bar{\gamma} = 3$, which allows an analytic potential, eq. (11) becomes the same as eq. (1), with

$$\gamma = 3 + \beta^{-1}. \quad (13)$$

If the asymptotic slope is steeper than the desired slope near and inside R_v , it could be partly compensated for by a proper choice of a lower value for c . Otherwise, a more accurate match in the outer regions may be helped by a deviation of $\bar{\gamma}$ from 3.

2.2.4 Slopes

The parameters α and $\bar{\gamma}$ (or γ) are the slopes in the asymptotic regions, which may fall well outside the radius range of interest, for example between $0.01R_v$ and R_v . For the slopes in points of interest, the slope profile of $\bar{\rho}(r)$ is $-\bar{s}(r)$, derived from eq. (3) to be

$$\bar{s}(r) = -\frac{d \log \bar{\rho}}{d \log r} = \frac{\alpha + \bar{\gamma} x^{1/\beta}}{1 + x^{1/\beta}}. \quad (14)$$

This allows one to express the slopes in specific regions of interest by the model parameters. Asymptotically, at $x \ll 1$ the slope corresponds to $\bar{s} = \alpha$ and at $x \gg 1$ it is $\bar{s} = \bar{\gamma}$. At $x = 1$, we have $\bar{s} = 0.5(\alpha + \bar{\gamma})$, reducing to $\bar{s} = 2$ (for $\bar{\rho}$, not ρ) when $\alpha + \bar{\gamma} = 4$ (e.g. $\alpha = 1$ and $\bar{\gamma} = 3$). Inverting eq. (14), a slope of $-\bar{s}$ is obtained by $\bar{\rho}(r)$ at

$$x_{-\bar{s}} = \left(\frac{\bar{s} - \alpha}{\bar{\gamma} - \bar{s}} \right)^\beta. \quad (15)$$

In particular, $\bar{s} = 2$, where the velocity curve is at a peak, is obtained at

$$x_{-2} = x_{\max} = \left(\frac{2 - \alpha}{\bar{\gamma} - 2} \right)^\beta. \quad (16)$$

This defines an alternative and more physical characteristic radius r_{\max} , which coincides with r_c for $\alpha + \bar{\gamma} = 4$. The corresponding alternative concentration parameter is

$$c_m = \frac{R_v}{r_{\max}} = \left(\frac{\bar{\gamma} - 2}{2 - \alpha} \right)^\beta c, \quad (17)$$

coinciding with c only for $\alpha + \bar{\gamma} = 4$.

The slope profile of $\rho(r)$ can be similarly derived from eq. (11). For example, for $\bar{\gamma} = 3$ it is

$$s(r) = \frac{\alpha + \gamma x^{1/\beta}}{1 + x^{1/\beta}}, \quad \gamma = \bar{\gamma} + \beta^{-1}. \quad (18)$$

While at $x \ll 1$ the asymptotic slope is α , the same as for $\bar{\rho}$, at $x \gg 1$ it is γ , which is steeper than the $\bar{\gamma} = 3$, and becomes somewhat closer to it for larger β . A slope of $s = 2$ for $\rho(r)$ is obtained in this case at

$$x_{-2} = \left(\frac{2 - \alpha}{\gamma - 2} \right)^\beta, \quad (19)$$

with γ replacing $\bar{\gamma}$ in eq. (16). This is $x = 1$ for $\alpha + \gamma = 4$. The slope of $\rho(r)$ deviates from the slope of $\bar{\rho}(r)$ by

$$\Delta s = s(r) - \bar{s}(r) = \frac{\beta^{-1} x^{1/\beta}}{1 + x^{1/\beta}}. \quad (20)$$

At $r = 0.015R_v$, with $c \sim 10$, typical in the fits to cuspy profiles, this deviation is only $\Delta s \sim 0.1$. With a larger c , and with a larger β , the deviation could be larger by a factor of $\sim 2 - 3$.

We will see in §4 that eq. (3), with a fixed β in the range 1–3, and especially with $\beta \sim 2$, provides excellent fits to simulated profiles, where α , c and $\bar{\gamma}$ are free. The challenge next is to obtain an explicit expression for the potential. This can be done for a general α with specific choices of β and $\bar{\gamma}$, as we show in §3.

2.2.5 Physical Meaning of the Parameters

The values of the parameters in the functional form of eq. (3), as obtained by a best fit to a simulated or observed target profile within a given radius range of interest, say $(0.01 - 1)R_v$, may not have an obvious physical meaning. For example, in some cases, the asymptotic slope α may be materialized only well below the minimum radius of interest, while the quantity of interest is the slope near this minimum radius, which can in principle be very different from α . Similarly, the value of c (namely r_c) may be hard to interpret, and in some cases c could be so large such that r_c is below the minimum radius of interest. Quantities of physical meaning are, for example, the slopes at the inner and outer radii of interest, say \bar{s}_1 and \bar{s}_2 at $r = 0.015R_v$ and at R_v , respectively, as well as the concentration parameter referring to the maximum velocity, c_m . These quantities are given as functions of the model parameters in eq. (14) and eq. (17). Note that a model that matches the target profile within the range of interest may in principle deviate from a real DM-halo profile outside this range, and in some cases be totally irrelevant there. The moral is that the best-fit model should not be extrapolated without care to outside the radius range within which the best fit was performed.

In order to demonstrate the possibly dubious physical meaning of the model parameters and how large the deviations outside the fitting range could be, one can estimate N best-fit parameters from N pairs of radii and the given slopes at these radii, $(r_{-\bar{s}}, \bar{s})$, in a target profile from simulations or observations. One can apply to each pair eq. (14) (or eq. (15)), e.g. in the form

$$c = \left(\frac{\bar{s} - \alpha}{\bar{\gamma} - \bar{s}} \right)^\beta \frac{R_v}{r_{-\bar{s}}}, \quad (21)$$

and solve the set of N equations for the free model parameters, c , α , and so on. As a simple example, we fix in the model $\bar{\gamma} = 3$ and β at either 1 or 2, and solve the corresponding set of two equations for a target with given \bar{s}_1 and $\bar{s}_2 = 2.3$ (typical in simulated haloes).

For a cusp of $\bar{s}_1 = 1$, the solution for $\beta = 1$ is $(\alpha, c) = (0.94, 1.9)$, namely α is close to the target inner slope but c is rather small, with r_c not much smaller than R_v . For a similar cusp but with $\beta = 2$ the solution becomes $(0.30, 8.2)$, namely α is very different from the target slope of $\bar{s}_1 = 1$, while the value of c is closer to what one expects from c_m or from concentrations obtained for the NFW profile.

For a core of $\bar{s}_1 = 0$, the solution for $\beta = 1$ is $(\alpha, c) = (-0.16, 3.5)$, and for $\beta = 2$ it is $(-2.5, 48)$. In the latter, α is very different from \bar{s}_1 and c is very large, making r_c not much larger than the minimum radius of interest $0.01R_v$. In this case, of fitting a core with $\beta = 2$, the value of α becomes even more negative and c becomes even larger when the constraint (R_v, \bar{s}_2) is replaced by $(r_{-\bar{s}_2}, 2)$ where the velocity peaks, which is typically at $r_{-\bar{s}_2}/R_v = 0.16$ in simulated haloes. Indeed, best fits to simulated profiles with cores, in §4, yield large negative α values and $c \sim 100$ or even larger. The same is true for $\beta = 2$ when $\bar{\gamma}$ is left free in the fit. In

this case, of $\beta = 2$ fitting a core, the profile at radii below $0.01R_v$ is unphysical, with a mean-density profile that is rising with radius encompassing a hole at very small radii. The virtue of such models with $\beta = 2$ is the excellent fit they provide in the range of interest to the variety of halo profiles, and their fully analytic nature when applied with $\bar{\gamma} = 3$ (see below).

3 ANALYTIC POTENTIAL AND DISPERSION

3.1 Special Cases with Fully Analytic Solutions

The density profile of eq. (1) has fully analytic expressions for the profiles of mass-velocity, potential and velocity dispersion in the special cases where $\beta = n$ and $\gamma = 3 + k/n$ with n and k natural numbers $(1, 2, \dots)$. The cases with $k = 1$ are equivalent to $\bar{\gamma} = 3$ in eq. (3) for any n . These expressions for general n and k are provided in detail in Zhao (1996), and are summarized in our appendix §A. Originally these profiles were meant to fit the stellar profiles of spheroidal galaxies, where there was no need to scale the radius by a variable r_c , or equivalently by a free concentration parameter c . In particular, a good fit is obtained to “classical” stellar spheroids by the special case $k = n = 1$, where the outer slope is rather steep, $\gamma = 4$, and the inner slope is free (Dehnen 1993; Tremaine et al. 1994). This case is analogous to eq. (3) with $\beta = 1$ and $\bar{\gamma} = 3$, except that we add a free concentration parameter c , which also helps dealing with the otherwise too steep outer slope in the context of DM haloes. For the purpose of DM haloes, where the outer slope is typically less steep than for spheroidal stellar systems, we restrict our attention here to two models of this family, both with $\bar{\gamma} = 3$ ($k = 1$), one with $n = 1$ ($\gamma = 4$), and the other with $n = 2$ ($\gamma = 3.5$). For any n , the lowest k guarantees that γ is the smallest, and for larger values of n γ gets smaller and closer to 3. However, $n \geq 3$ correspond to shapes that do not match DM halo profiles.

For $k = 1$ and a general n , the density profile is

$$\rho(r) = \frac{\rho_c}{x^\alpha (1 + x^{1/n})^{n(3+1/n-\alpha)}}. \quad (22)$$

The mean-density profile is

$$\bar{\rho}(r) = \frac{\bar{\rho}_c}{x^\alpha (1 + x^{1/n})^{n(3-\alpha)}}, \quad (23)$$

namely as in eq. (1) and eq. (3) with $\beta = n$ and $\bar{\gamma} = 3$, and with $3\rho_c = (3 - \alpha)\bar{\rho}_c$. The mass, velocity and force profiles are given in eqs. (6) to (8), with $\bar{\rho}_c$ and μ from eq. (4) and eq. (5), substituting $\beta = n$ and $\bar{\gamma} = 3$. Recall that the outer asymptotic slope for $\bar{\rho}$ is $\bar{\gamma} = 3$ for any n , while the asymptotic slope for ρ is $\gamma = 3 + 1/n$.

3.2 Two-parameter Potential for $\bar{\gamma} = 3$ and $\beta = 1$

Here we fix $n = 1$, so with $k = 1$ the density profiles are simply

$$\rho(r) = \frac{\rho_c}{x^\alpha (1+x)^{4-\alpha}}, \quad \bar{\rho}(r) = \frac{\bar{\rho}_c}{x^\alpha (1+x)^{3-\alpha}}, \quad (24)$$

With one free parameter, α , this resembles elliptical galaxies. With two free parameters, α and c , we will see in §4 that this function provides reasonable matching to simulated profiles in the inner DM halo, though with possible $\sim 10\%$ deviations in the middle halo. The mass, velocity and force profiles are given in eqs. (3) to (8) with $\bar{\gamma} = 3$ and $\beta = 2$.

The potential is obtained by integration of the force over radius. We assume that the halo density profile is truncated at a certain radius R_t (which could be $\sim R_v$ or larger, as desired). The potential at $r \leq R_t$, defined to vanish at infinity, is given by

$$U(r) = - \int_r^{R_t} \frac{M(y)}{y^2} dy - \int_{R_t}^{\infty} \frac{R_t}{y^2} dy. \quad (25)$$

Denoting $c_t = (R_t/R_v)c$, $V_t = V(R_t)$ and $R_t = M(R_t)$ from eq. (7) and eq. (6) with $\bar{\gamma} = 3$ and $\beta = 1$, one obtains

$$U(r) = -V_t^2 + \frac{c\mu}{(2-\alpha)} V_v^2 \times \left[\left(\frac{x}{1+x} \right)^{2-\alpha} - \left(\frac{c_t}{1+c_t} \right)^{2-\alpha} \right], \quad (26)$$

where μ is given by eq. (5) for $\bar{\gamma} = 3$ and $\beta = 1$. The second term in the square brackets ensures that $U(R_t) = -V_t^2$, and the normalization factor in front of the square brackets guarantees that $dU/dr = -F(r)$. If the halo mass extends well beyond the virial radius, $c_t \gg 1$, the potential approaches

$$U(r) \simeq \frac{c\mu}{(2-\alpha)} \left[\left(\frac{x}{1+x} \right)^{2-\alpha} - 1 \right] V_v^2. \quad (27)$$

Note that the potential as quoted in eq. (A7) is for $R_t \rightarrow \infty$.

The velocity dispersion can be obtained under the assumption that the phase-space distribution function depends only on energy, namely that the velocity dispersion tensor is isotropic. The radial velocity dispersion has to satisfy the Jeans equation (or hydrostatic equation), namely

$$\frac{d(\rho\sigma_r^2)}{dr} = -\rho \frac{dU}{dr}. \quad (28)$$

If one assumes that $R_t \rightarrow \infty$ and the boundary condition is $\rho\sigma_r^2 = 0$ as $r \rightarrow \infty$, one can obtain the velocity dispersion by performing the integral

$$\sigma_r^2(r) = \frac{1}{\rho(r)} \int_r^{\infty} \frac{M(y)\rho(y)}{y^2} dy. \quad (29)$$

This integral is expressed analytically in eq. (A10) following Zhao (1996). Already for $n = k = 1$ it involves a sum of five terms, which we therefore avoid spelling out here. Explicit expressions for this case are given in equations 7-11 of Tremaine et al. (1994).

3.3 Two-parameter Potential for $\bar{\gamma} = 3$ and $\beta = 2$

We will see in §4 that among the family of analytic profiles the case $k = 1$ with $n = 2$ provides the most natural match to the shape of simulated DM profiles, with only two free parameters, α and c . The density profiles are

$$\rho(r) = \frac{\rho_c}{x^\alpha (1+x^{1/2})^{2(3.5-\alpha)}}, \quad (30)$$

$$\bar{\rho}(r) = \frac{\bar{\rho}_c}{x^\alpha (1+x^{1/2})^{2(3-\alpha)}}. \quad (31)$$

The mass, velocity and force profiles are given in eqs. (3) to (8) with $\bar{\gamma} = 3$ and $\beta = 2$.

The potential, based on eq. (A7) but assuming that the density profile is truncated at $R_t = (c_t/c)R_v$, is

$$U(r) = -V_t^2 - 2c\mu V_v^2 \times \left(\frac{\chi_{c_t}^{2(2-\alpha)} - \chi^{2(2-\alpha)}}{2(2-\alpha)} - \frac{\chi_{c_t}^{2(2-\alpha)+1} - \chi^{2(2-\alpha)+1}}{2(2-\alpha)+1} \right), \quad (32)$$

where

$$\chi(x) = \frac{x^{1/2}}{1+x^{1/2}}, \quad \chi_{c_t} = \chi(x=c_t). \quad (33)$$

The term involving $\chi(c_t)$ ensures that $U(R_t) = -V_t^2$, and the normalization factor in front of the big brackets guarantees that $dU/dr = -F(r)$.

An analytic expression for the velocity dispersion profile can be obtained from eq. (A10). It is an elaborate sum of many terms, which we avoid spelling out here.

3.4 Three-Parameter Double Profiles

Any linear combination of the analytic profiles will naturally also have an analytic potential, and with more free parameters the fit to simulations can be made as good as desired.³ We will see that this may not be necessary for a fit of the $\beta = 2$ model in the range $(0.01 - 1)R_v$, but it may be useful for the $\beta = 1$ model if an excellent fit is desired at all radii in this range. The simplest option is a sum of two $\bar{\gamma} = 3$ profiles with the same α and β but different concentrations, c_1 and c_2 , namely three free parameters. The number of free parameters is the same as in the single profile of eq. (3) with β fixed and $\bar{\gamma}$ free, and we will see that the quality of the fit is also similar, except that for the double profile we also have an analytic potential.

We adopt the linear combination

$$\bar{\rho}(r) = \frac{\bar{\rho}_{c,1}}{x_1^\alpha (1+x_1^{1/n})^{n(3-\alpha)}} + \frac{\bar{\rho}_{c,2}}{x_2^\alpha (1+x_2^{1/n})^{n(3-\alpha)}}, \quad (34)$$

where $x_i = c_i r/R_v$ for $i = 1, 2$. With the choice $c_1 > c_2$, the first and second terms are made to dominate the

³ Schaller et al. (2015) successfully used a linear combination of two functions for ρ , while here we use such a combination for $\bar{\rho}$, keeping the analytic nature of the profiles.

inner and outer halo, respectively. The value of α for the second component may be less important, so we let it be the same as α of the first component, thus keeping the number of free parameters at three. The normalization coefficients $\bar{\rho}_{c,i}$ are determined such that the fractional contribution of each component to $\bar{\rho}$ at R_v is f_i ($f_1 + f_2 = 1$), namely

$$\bar{\rho}_{c,i} = f_i \bar{\rho}_v c_i^\alpha (1 + c_i)^{3-\alpha}. \quad (35)$$

The values of f_i are to be decided in advance, before the functional form is used to match different simulated or observed profiles, so they should not be regarded as additional free parameters. In order to chose fiducial values for f_i , we perform in §4 experimental fits to simulated profiles where we do allow f_i to vary. We find that best fits to $\bar{\rho}(r)$ are obtained with f_1 in the range 0.1 – 0.5, and therefore adopt hereafter $f_1 = 0.33$ and $f_2 = 0.67$ as our fiducial fixed values. We also note that the choice $f_1 = f_2 = 0.5$ works slightly better when fitting $\rho(r)$ rather than $\bar{\rho}(r)$. As long as f_1 is comparable to or slightly smaller than f_2 , their exact values do not make a significant difference and should be regarded as fine tuning.

The associated profiles of local density, mass, velocity squared, force, potential and velocity-dispersion squared are all analogous sums of two components. The slope of $\bar{\rho}(r) = \bar{\rho}_1(r) + \bar{\rho}_2(r)$ becomes

$$\bar{s}(r) = \frac{\bar{\rho}_1(r) \bar{s}_1(r) + \bar{\rho}_2(r) \bar{s}_2(r)}{\bar{\rho}(r)}, \quad (36)$$

where $\bar{s}_i(r)$ are given in eq. (14) for the respective x_i with $\bar{\gamma} = 3$ and $\beta = 1$ or 2.

4 FIT TO SIMULATIONS

4.1 The Simulations

4.1.1 General

We use here three pairs of haloes from the NIHAO suite of zoom-in cosmological simulations (Wang et al. 2015) at $z = 0$. The simulations are described, e.g., in Tollet et al. (2016); Dutton et al. (2016a). Each pair consists of simulations with and without baryons (“HYDRO” and “DMO” respectively), otherwise starting from the same initial conditions. The six haloes thus span a range of profiles with a variety of inner cusps and cores. The resolution allows an accurate recovery of the density profile at $(0.01 - 0.02)R_v$, where the evolution between cusp and core is most pronounced.

The standard flat Λ CDM cosmology was assumed, with the Planck parameters (Ade et al. 2014) ($H_0 = 67.1 h^{-1} \text{Mpc}$, $\Omega_m = 0.3175$, $\Omega_\Lambda = 1 - \Omega_m = 0.6825$, $\Omega_b = 0.0490$, $\sigma_8 = 0.8344$, $n = 0.9624$).

The simulations were performed using the SPH code GASOLINE (Wadsley, Stadel & Quinn 2004), as modified by Keller et al. (2014) to reduce the formation of blobs and improve mixing. The treatment of cooling via hydrogen, helium and metal-lines in a uniform ultraviolet ionizing background is described in Shen, Wadsley & Stinson (2010). The star formation

recipe is described in Stinson et al. (2006). The thermal stellar feedback, which is the main driver of evolution in the inner-halo profile, includes an early phase of winds and photoionization from massive stars, and a later epoch starting 4 Myr after the star formation, when the first supernovae explode and dominate the feedback thereafter. The Chabrier (2003) IMF is used. Stars in the mass range $(8 - 40)M_\odot$ eject an energy of 10^{51} erg and metals into the interstellar medium surrounding stars. Supernova feedback is implemented using the blast-wave formalism described in Stinson et al. (2006). To avoid rapid radiative cooling in the dense gas receiving the energy, cooling of gas particles inside the blast region is delayed for ~ 30 Myr.

The DM haloes were identified using the MPI+OpenMP hybrid halo finder AHF⁴ (Knollmann & Knebe 2009; Gill, Knebe & Gibson 2004). AHF locates local over-densities in an adaptively smoothed density field as prospective halo centers. The virial masses of the haloes are defined as the masses within a sphere containing $\Delta_v = 200$ times the cosmic critical matter density, $\rho_{\text{crit}} = 3H(z)^2/8\pi G$.

The galaxies produced in the NIHAO simulations match the main observational constraints, including the Tully-Fisher relation, the stellar to halo mass ratio, the main sequence of star-forming galaxies (Wang et al. 2015, 2017), outflows through the CGM and metallicity (Gutcke et al. 2017), the presence of bulge-less disks (Obreja et al. 2016), the velocity function of “too big to fail” dwarf galaxies (Dutton et al. 2016b), and the presence of a wide range of inner-halo profiles ranging from cusp to core (Tollet et al. 2016; Dutton et al. 2016a). This is encouraging in terms of the potential validity of the star-formation and feedback subgrid recipes and the resultant DM density profiles in the inner halo. Our only concern here is that the six simulated profiles are representative of the variety of real halo profiles.

4.1.2 Measuring the Profiles

The mass profile is obtained by sorting the DM particles by their distance from the halo center, yielding a rather smooth mass profile. The mass profile is binned into points equally spaced in $\log r$, with spacing of 1/35 dex, namely about 70 points in the range of interest $(0.01 - 1)R_v$. The profiles of $\bar{\rho}(r)$ and $V(r)$ are computed straightforwardly at these grid points. The local density profile $\rho(r)$ is obtained by a smooth derivative of the mass profile using a Savitzky-Golay filter (Savitzky & Golay 1964), with a second-degree polynomial and a window size of ~ 10 bins. The smoothing is applied beyond the radius range of interest to avoid edge effects. The logarithmic slope profiles of $\bar{\rho}$ and ρ are obtained by similar smooth derivatives using the same filter.

We consider the safe, reliable and interesting range of the profiles to be $(0.01 - 1)R_v$, but also show extended profiles from the simulations below $0.01R_v$ and out to

⁴ <http://popia.ft.uam.es/AMIGA>

$2R_v$. The actual gravitational softening radius of the simulation is typically a factor 2–3 smaller than $0.01R_v$, and the choice of $0.01R_v$ as a safe convergence radius for the NIHAO simulations is justified in Tollet et al. (2016, section 2.4).

4.2 Fitting the Simulations

4.2.1 Method

We use the 3x2 simulated haloes at $z = 0$ to evaluate the ability of the new analytic profiles to match the variety of realistic halo profiles, especially in the inner halo, and to rank the relative goodness of fit among these profiles. The halo masses in the hydro simulations are 2.7×10^{10} , 1.3×10^{11} and $9.4 \times 10^{11} M_\odot$.⁵ We refer here to the simulations according to their log halo masses, namely 10D, 11D and 12D for the DMO simulations and 10H, 11H and 12H for the hydro simulations.

In all cases, the DMO profiles are cuspy, $\bar{s}_1 \simeq 1.1 - 1.4$, and can be well fit by the NFW profile and especially by the Einasto profile. Their response to gas inflow and outflow is described in Tollet et al. (2016). In the high-mass halo 12H, where feedback-driven outflows are negligible (producing a relatively high stellar-to-halo mass ratio $M_s/M_v = 4.75 \times 10^{-2}$), the baryons lead to a contraction of the inner halo and thus to a steepening of the inner cusp in the halo density profile of the hydro simulation, from $\bar{s}_1 = 1.1$ to 1.3. In the intermediate-mass halo 11H, where there are intense episodes of inflow, partly recycled, and the feedback-driven outflows are very effective (yielding a lower $M_s/M_v = 7.08 \times 10^{-3}$), the baryons lead to a significant expansion of the inner halo, flattening the cusp to a core in the hydro simulation, from $\bar{s}_1 = 1.3$ to 0.2. In the low-mass halo, where gas ejection is efficient and it suppresses the inflow such that the SFR becomes lower (with a very low $M_s/M_v = 1.78 \times 10^{-3}$), the baryons lead to a weaker expansion, and a partial flattening of the cusp, from $\bar{s}_1 = 1.4$ to 0.6.

We note in the example simulations shown below that in the DMO simulations the profile of the *slope* of $\bar{\rho}(r)$ in $(0.01 - 1)R_v$ is well fit by a power law, indicating that the Einasto profile will be a good fit. However, the slope profiles in the hydro simulations tend to deviate from a power law, so the Einasto profile is not expected to be a good fit.

We fit each of the new analytic functional forms discussed in the previous two sections to each of the simulated profiles. The fit is performed on the binned profile of $\bar{\rho}$ with no further smoothing. The fitting method is Levenberg-Marquardt least squares (Levenberg 1944; Marquardt 1963). The rms of the residuals of $\log \bar{\rho}$, denoted Δ , is used to evaluate a *relative* global goodness of fit. The absolute value of Δ is sensitive to how smooth the target simulated profile is (namely the resolution of

the simulations and the binning procedure for the profile), so it should mostly serve for comparing the performance of different models in fitting target profiles that were measured in the same way rather than for an absolute goodness of fit.

The binning is important in order to allow us to focus the fit on a desired specific radius range, such as the cusp-core region, while still obtaining a sensible fit in other regions. With the bins equally spaced in log radius, the effective weight assigned to the inner halo is larger than it would have been in a maximum-likelihood fit performed with equal weights to each particle. When we wish to assign an enhanced weight to a given region, we may assign enhanced weights, by a factor w , to the data points in bins that lie in this region. The value of w is decided in advance according to the focus of the study, e.g., $w = 1$ when an overall accurate fit is desired, or $w > 1$ in the inner halo when the focus is on the cusp-core region. This weighting procedure makes only a minor difference. We should stress again that the binning and the nonuniform weighting allow only a relative goodness-of-fit estimate, not an absolute one.

4.2.2 Summary of Fit Results

The results of the fits of the 6 models to the 6 target simulated profiles with uniform weights ($w = 1$) are summarized in Table 1. The fits of the three models with $\beta = 2$ are shown in Figs. 1 to 3, and the analogous models with $\beta = 1$ are shown in Figs. B1 to B3. In §C we bring the equivalent table and figures for fits with a high weight of $w = 10$ at $r = (0.01 - 0.03)R_v$, the most interesting region of cusp-to-core transition.

The table lists the haloes in columns and the models in rows. The haloes are marked 1 to 6, ordered by the inner slope \bar{s}_1 at $0.015R_v$ from steep to flat, which is quoted. The crude halo masses and D or H help identifying the haloes, from the DMO and hydro simulations respectively. The models, each in two versions with $\beta = 1$ and 2, are (a) the three-parameter free- $\bar{\gamma}$ model with maximum flexibility and mass-velocity analytic profiles, (b) the two-parameter $\bar{\gamma} = 3$ model with analytic potential, and (c) the three-parameter double model with $\bar{\gamma} = 3$ and an analytic potential.

The entries for each model-halo pair are first of all two estimates of the goodness of fit (in bold face): Δ is the overall rms of log residuals of $\bar{\rho}(r)$ in the range $(0.01 - 1)R_v$, and $\Delta\bar{s}_1$ is the deviation of the inner slope \bar{s}_1 in the model from the simulated halo profile. Then, quoted in the left column are the values of the best-fit parameters of the functional form (e.g., c , α and $\bar{\gamma}$), and in the right column the values of the parameters with physical meaning (c_m , \bar{s}_1 , and \bar{s}_2 - the slope at R_v). The best fitting model in terms of Δ or $\Delta\bar{s}_1$ for each halo (namely in each column) is marked by an underline.

The fits are in general quite good, with the rms log residual $\Delta \sim 0.01$, ranging from below one percent to a few percent. The model inner slope matches the true value with deviations $\bar{s}_1 \sim 0.1$, ranging from 0.01 to 0.4. For $\beta = 2$ typically $\Delta \lesssim 0.01$ and $\bar{s}_1 \lesssim 0.1$.

For the cusped haloes, no. 1 to 4, the best-fit models

⁵ These simulated galaxies are termed in (Wang et al. 2015) g2.63e10, g2.19e11 and g8.06e11, respectively, referring to the halo masses from the low-resolution box from which the haloes were chosen.

halo #		1	2	3	4	5	6							
name		10D	11D	12H	12D	10H	11H							
\bar{s}_1		1.4	1.3	1.3	1.1	0.6	0.2							
#	model	params												
a1	$\bar{\gamma}$ free, $\beta = 1$	Δ $\Delta\bar{s}_1$	0.008 0.08	0.010 0.12	0.012 0.12	0.018 0.16	0.008 0.08	0.008 0.08	0.008 0.08	0.008 0.08	0.008 0.08	0.008 0.08	0.008 0.08	0.008 0.08
		c c_m	7.6 8.3	7.6 5.5	23.4 8.3	6.2 4.2	26.6 7.1	21.6 4.6	21.6 4.6	21.6 4.6	21.6 4.6	21.6 4.6	21.6 4.6	21.6 4.6
		α \bar{s}_1	1.3 1.5	1.3 1.4	1.1 1.4	1.1 1.3	-0.1 0.7	-0.6 0.1	-0.6 0.1	-0.6 0.1	-0.6 0.1	-0.6 0.1	-0.6 0.1	-0.6 0.1
		$\bar{\gamma}$ \bar{s}_2	2.7 2.6	2.5 2.4	2.3 2.3	2.6 2.4	2.5 2.4	2.6 2.4	2.6 2.4	2.6 2.4	2.6 2.4	2.6 2.4	2.6 2.4	2.6 2.4
a2	$\bar{\gamma}$ free, $\beta = 2$	Δ $\Delta\bar{s}_1$	0.005 0.03	0.007 0.09	0.010 0.08	0.014 0.12	0.003 0.01	0.012 -0.14						
		c c_m	6.2 8.3	6.4 5.2	328 8.3	3.4 3.9	442 6.6	157 4.3	157 4.3	157 4.3	157 4.3	157 4.3	157 4.3	157 4.3
		α \bar{s}_1	0.9 1.4	0.8 1.4	-1.1 1.4	0.7 1.2	-5.2 0.6	-4.5 0.1	-4.5 0.1	-4.5 0.1	-4.5 0.1	-4.5 0.1	-4.5 0.1	-4.5 0.1
		$\bar{\gamma}$ \bar{s}_2	3.3 2.6	3.0 2.4	2.5 2.3	3.3 2.4	2.9 2.5	3.1 2.5	3.1 2.5	3.1 2.5	3.1 2.5	3.1 2.5	3.1 2.5	3.1 2.5
b1	$\bar{\gamma} = 3$, $\beta = 1$	Δ $\Delta\bar{s}_1$	0.015 0.16	0.020 0.24	0.031 0.37	0.022 0.26	0.041 0.42	0.042 0.25						
		c c_m	3.6 7.3	2.2 4.2	1.8 4.9	2.5 3.7	6.0 5.4	7.2 4.1	7.2 4.1	7.2 4.1	7.2 4.1	7.2 4.1	7.2 4.1	7.2 4.1
		α \bar{s}_1	1.5 1.6	1.5 1.5	1.6 1.7	1.3 1.4	0.8 1.0	0.2 0.5	0.2 0.5	0.2 0.5	0.2 0.5	0.2 0.5	0.2 0.5	0.2 0.5
		\bar{s}_2	2.7	2.5	2.5	2.5	2.7	2.7	2.7	2.7	2.7	2.7	2.7	2.7
b2	$\bar{\gamma} = 3$, $\beta = 2$	Δ $\Delta\bar{s}_1$	0.009 -0.03	0.007 0.08	0.018 0.24	0.015 0.07	0.008 0.09	0.012 -0.17						
		c c_m	22.9 9.5	6.7 5.2	4.4 6.4	9.2 4.2	123 6.2	238 4.3	238 4.3	238 4.3	238 4.3	238 4.3	238 4.3	238 4.3
		α \bar{s}_1	0.4 1.4	0.8 1.4	1.1 1.5	0.5 1.2	-2.5 0.7	-5.6 0.0	-5.6 0.0	-5.6 0.0	-5.6 0.0	-5.6 0.0	-5.6 0.0	-5.6 0.0
		\bar{s}_2	2.6	2.4	2.4	2.4	2.5	2.5	2.5	2.5	2.5	2.5	2.5	2.5
c1	x2 $\bar{\gamma} = 3$, $\beta = 1$	Δ $\Delta\bar{s}_1$	0.005 0.04	0.008 0.11	0.012 0.16	0.015 0.13	0.006 0.02	0.011 -0.13						
		c_1 c_m	11.2 8.9	7.3 5.2	9.6 8.3	7.3 4.2	26.7 6.6	23.2 3.8	23.2 3.8	23.2 3.8	23.2 3.8	23.2 3.8	23.2 3.8	23.2 3.8
		c_2 \bar{s}_1	2.5 1.4	1.3 1.4	0.9 1.4	1.6 1.2	5.0 0.6	5.7 0.1	5.7 0.1	5.7 0.1	5.7 0.1	5.7 0.1	5.7 0.1	5.7 0.1
		α \bar{s}_2	1.2 2.6	1.2 2.4	1.2 2.3	1.1 2.4	-0.3 2.6	-0.9 2.6	-0.9 2.6	-0.9 2.6	-0.9 2.6	-0.9 2.6	-0.9 2.6	-0.9 2.6
c2	x2 $\bar{\gamma} = 3$, $\beta = 2$	Δ $\Delta\bar{s}_1$	0.009 -0.03	0.007 0.07	0.010 0.04	0.015 0.07	0.006 0.03	0.012 -0.17						
		c_1 c_m	22.9 9.5	16.9 5.2	313 7.3	9.2 4.2	5.2e4 6.2	237 4.3	237 4.3	237 4.3	237 4.3	237 4.3	237 4.3	237 4.3
		c_2 \bar{s}_1	22.9 1.4	5.9 1.3	29.7 1.3	9.2 1.2	1.5e4 0.6	238 0.0	238 0.0	238 0.0	238 0.0	238 0.0	238 0.0	238 0.0
		α \bar{s}_2	0.4 2.6	0.6 2.4	-2.2 2.4	0.5 2.4	-62.3 2.5	-5.6 2.5	-5.6 2.5	-5.6 2.5	-5.6 2.5	-5.6 2.5	-5.6 2.5	-5.6 2.5

Table 1. A summary of the fits of six models to the six simulated haloes. The haloes are ordered by the slope \bar{s}_1 at $0.015R_v$. The models, with $\beta = 1, 2$, are (a) the three-parameter flexible model with free $\bar{\gamma}$, (b) the analytic model with $\bar{\gamma} = 3$ and two free parameters, and (c) the double model with $\bar{\gamma} = 3$ and three free parameters. The quality of the fit is estimated by Δ and $\Delta\bar{s}_1$ (in bold face), the rms log residuals in $(0.01 - 1)R_v$ and the deviation of \bar{s}_1 from the simulated value. The other entries are the free parameters of the functional form (c , α , $\bar{\gamma}$) and the associated physical parameters (c_m , related to the velocity maximum, and \bar{s}_1 and \bar{s}_2 , the slopes at $0.015R_v$ and at R_v). The best fit in every column is marked by an underline.

are with $\beta = 2$. The three-parameter models a2 and c2 are naturally slightly better in most cases, but the two-parameter model b2 is comparable in two haloes and not far behind in the other two. The best fit for the semi-cored halo #5 is by model a2, and the best fit to the cored halo #6 is actually by model a1, with $\beta = 1$.

Overall, when an analytic potential is required, namely $\bar{\gamma} = 3$, best accuracy is provided by model c2, namely with $\beta = 2$ and three free parameters. However, for simplicity, model b2 provides fits that are comparable and almost as accurate, with only two free parameters (and $\beta = 2$). For the most accurate fits without a requirement for an analytic potential, the models with free $\bar{\gamma}$ provide slightly better fits, and better with $\beta = 2$ than $\beta = 1$, except for the cored halo. When an extremely accurate fit is desired, and only the velocity-mass profile is required to be analytic, one can appeal to the similar model with a free β .

When an enhanced weight is assigned to the core-cusp region, $w = 10$, we see in Table C1 that the fit of the inner slope is naturally better, with $\Delta\bar{s}_1$ values typically ranging from 0.00 to 0.05 compared to 0.01 – 0.24 with $w = 1$. This is at the expense of the overall fit, which is typically of comparable or lower quality with

respect to the $w = 1$ case, sometimes by a factor of ~ 2 in Δ .

While the values of the free parameters in the functional form vary significantly from model to model for the same halo, the physical parameters robustly characterize each halo independently of the model used. For example, c_m typically varies by less than $\pm 10\%$ from model to model for a given halo. The values of \bar{s}_1 and \bar{s}_2 typically vary by less than ± 0.1 for a given halo. Among the haloes, the values of c_m vary from 3.8 to 9.5, and they are weakly correlated with the inner slope \bar{s}_1 . The outer slope of $\bar{\rho}(r)$ at R_v is robust at $\bar{s}_2 = 2.5 \pm 0.1$.

Figures 1 to 3 show the best fits of the three models with $\beta = 2$ to the simulated profiles, focusing on the range $(0.01 - 1)R_v$. The analogous models with $\beta = 1$ are shown in Figs. B1 to B3. We show here results with uniform weights, $w = 1$, while in §C we show examples with $w = 10$ at $r = (0.01 - 0.03)R_v$, the most interesting region of cusp-to-core transition. Shown are the profiles of mean density $\bar{\rho}(r)$, local density $\rho(r)$, circular velocity $V(r)$, and mean-density slope $\bar{s}(r)$. The best-fit values of the free parameters, and the two measures of quality of fit, same as in Table 1, are quoted in the figures. We discuss these figures here.

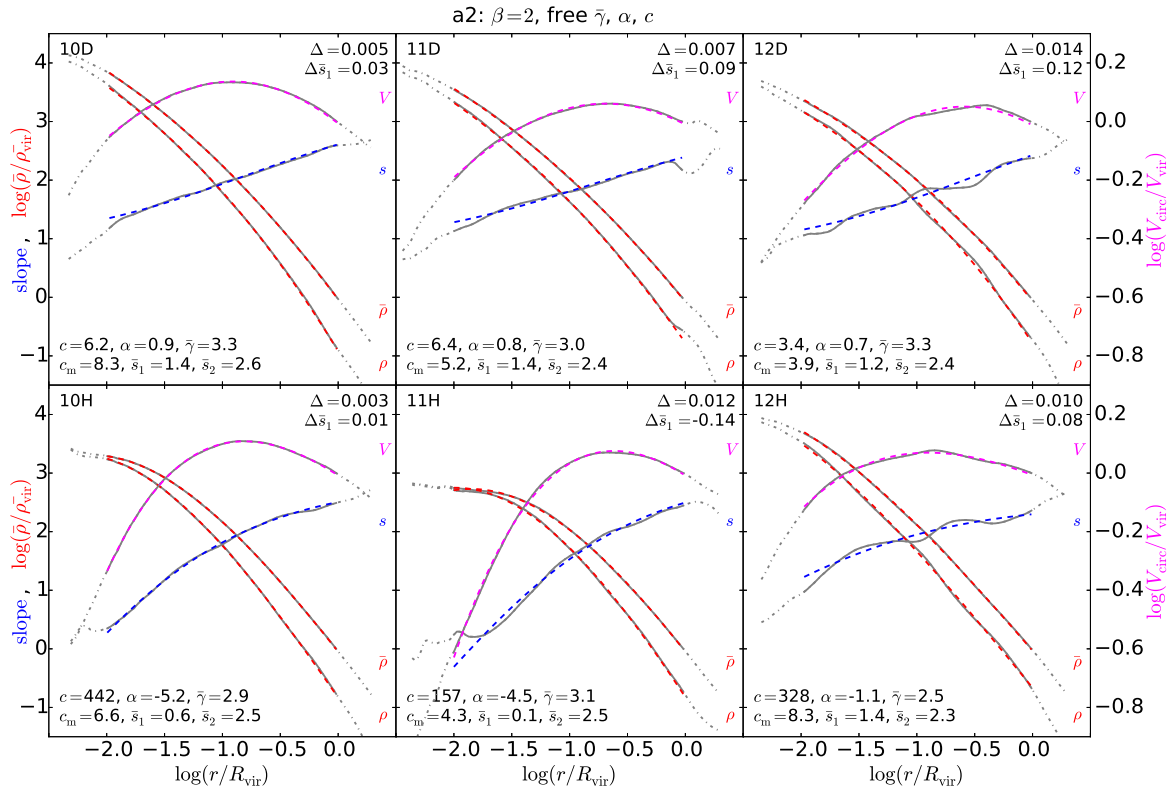


Figure 1. Best-fit model (dashed) versus the simulated profiles (solid). Shown are the profiles of $\bar{\rho}$, ρ , V and the $\bar{\rho}$ slope \bar{s} . This figure is for the flexible model a2, with $\bar{\gamma}$ free and $\beta = 2$ (three free parameters). The fits are excellent, with $\Delta = 0.003 - 0.014$ dex and $\Delta\bar{s}_1 = 0.01 - 0.14$. Figure B1 shows the same for model a1, with $\beta = 1$, where the fits are slightly less good, except for halo 11H with the flat core.

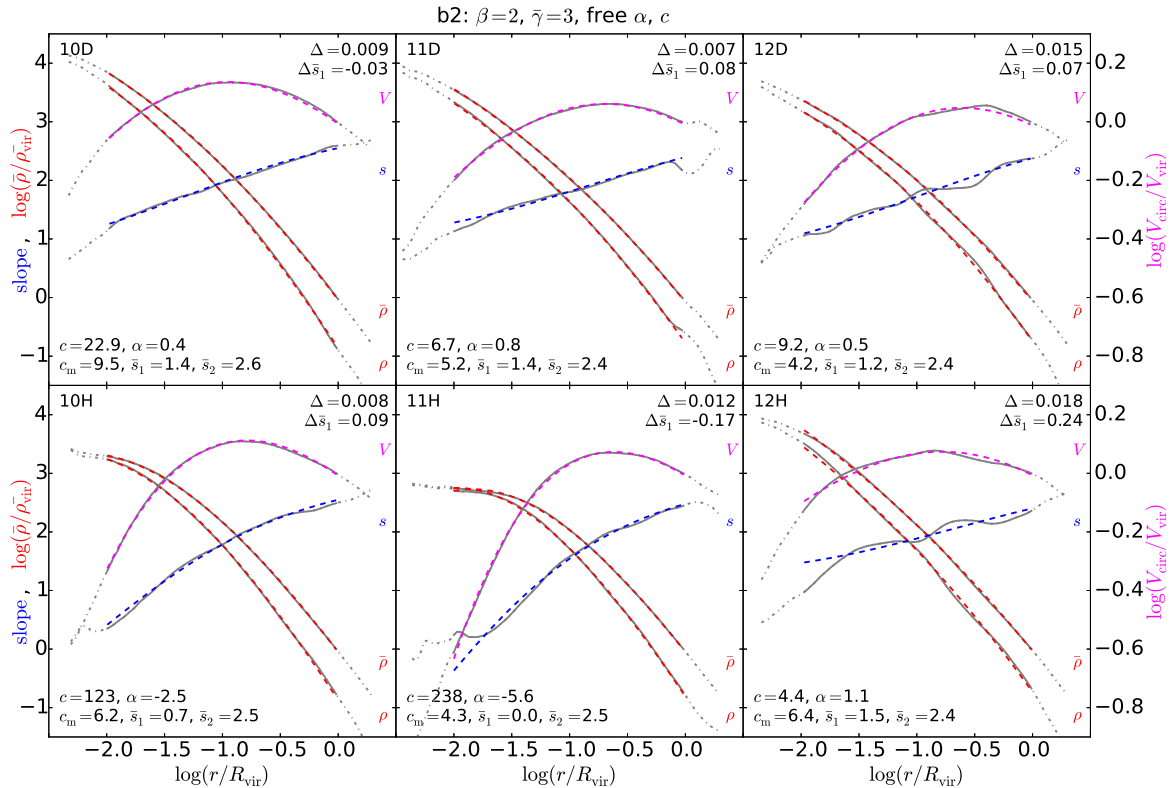


Figure 2. Same as Fig. 1 but for the fully analytic model b2, where $\bar{\gamma} = 3$ and $\beta = 2$ (two free parameters). The fit is still excellent, with $\Delta = 0.007 - 0.018$ dex and $\Delta\bar{s}_1 = 0.03 - 0.24$. Figure B2 shows the same for model b1, with $\beta = 1$, where the fits are less good for all haloes.

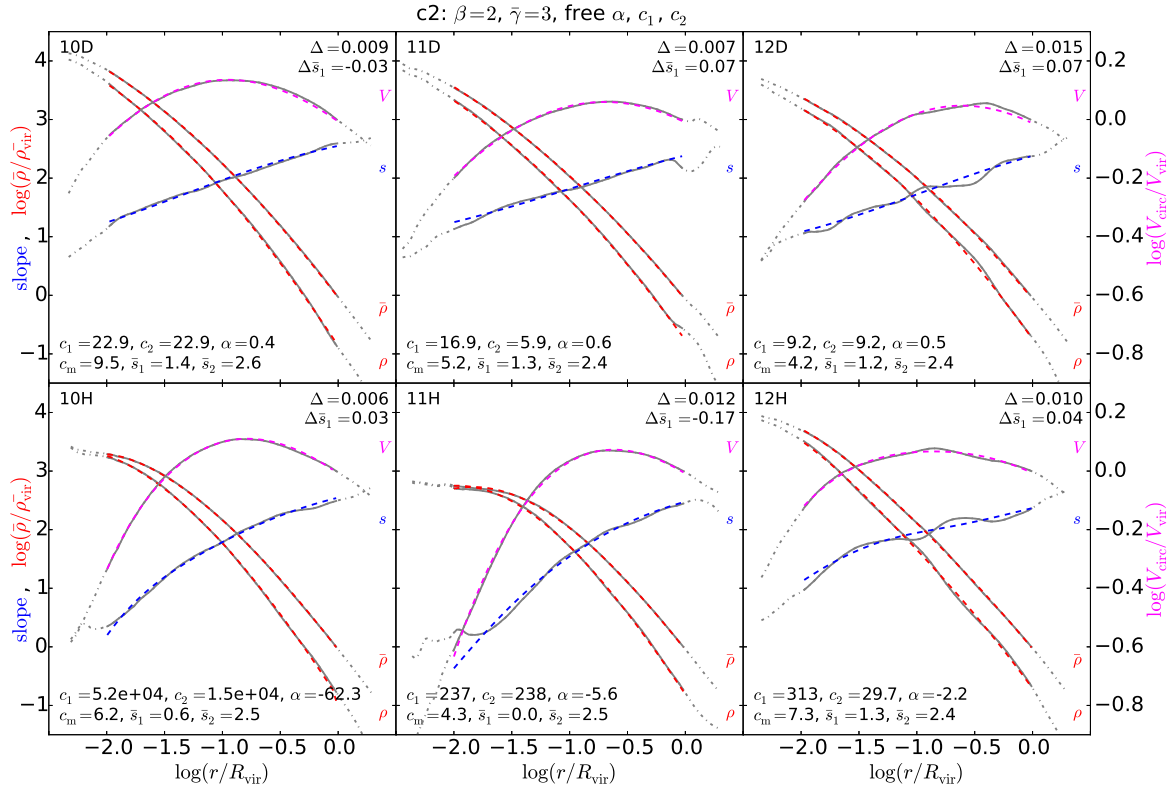


Figure 3. Same as Fig. 1 but for the fully analytic double model c2, where $\bar{\gamma} = 3$ and $\beta = 2$ (three free parameters). The fit is excellent, with $\Delta = 0.006 - 0.015$ dex and $\Delta\bar{s}_1 = 0.03 - 0.17$. Figure B3 shows the same for model c1, with $\beta = 1$, where the fits are comparable.

4.2.3 Free- $\bar{\gamma}$ Profiles with $\beta = 1, 2$, Models a1 and a2

Figures 1 and B1 refer to the three-parameter flexible model of §2.2, eq. (3), with the outer slope $\bar{\gamma}$ free, in addition to α and c . Recall that this model has analytic expressions for the density and mass-velocity profiles but not for the potential profile. For illustrative purposes we fix β at either 1 or 2, though any value of β can be used here.

The fits are excellent at all radii in all cases for the two values of β . The rms deviations within $(0.01 - 1)R_V$ are $\Delta = 0.003 - 0.014$ dex for $\beta = 2$ and $\Delta = 0.008 - 0.018$ dex for $\beta = 1$. The inner slope deviations are $\Delta\bar{s}_1 = 0.01 - 0.14$ and $0.08 - 0.16$ respectively. We learn that $\beta = 2$, in general, provides better fits than $\beta = 1$.

As expected, the useful parameters for characterizing the cusp-core are \bar{s}_1 (not α) and to a certain extent c_m (though it involves α and $\bar{\gamma}$). The values of \bar{s}_1 are in the range $1.4 - 0.1$, while α ranges from 0.9 to large negative values that have no physical interpretation. The values of c_m are limited to the relatively narrow range $3.9 - 8.3$, while the values of c can become extremely large, and therefore lack a physical meaning. The values of \bar{s}_{R_V} for model a2 are stable in the narrow range $2.3 - 2.6$, while the values of $\bar{\gamma}$ are somewhat larger and they span a broader range, $2.5 - 3.3$.

We conclude that the three-parameter model with free $\bar{\gamma}$ and $\beta = 2$ can be very useful in matching the profiles in all cases, where analytic density and mass-velocity profiles are desired but an analytic potential is not required. This function may be useful in particular

for the study of the outer profile, near and outside R_V , which could be affected by tides as a function of the halo environment and is expected to vary with the accretion rate onto the halo (Diemer & Kravtsov 2014).

4.2.4 Analytic Profiles with $\bar{\gamma} = 3$, Models b1 and b2

Figure 2 and Fig. B2 refer to the simple, two-parameter, $\bar{\gamma} = 3$, fully analytic models b2 and b1, with $\beta = 2$ and $\beta = 1$ respectively. The free parameters are α and c . Model b1 has a somewhat simpler analytic expression for the potential, and a much simpler expression for the velocity dispersion, but model b2 is a better fit to the simulated haloes, and we therefore focus on it here.

The profile with $\beta = 2$ turns out to more naturally match the shape of the simulated profiles in the middle halo, both for the cases of cusps and cores. In particular, it allows to capture the non-power-law slope profile in the cases of a core, and the slopes near R_V . The fit for $\beta = 2$ has $\Delta \sim 0.007 - 0.018$ and $\Delta\bar{s}_1 = 0.03 - 0.24$. This is excellent, though naturally not as good as the three-parameter model a2.

As expected in §2.2.5, with $\beta = 2$ the values of the parameters α and c are not meaningful for the radius range of interest (this is true for models a2 and c2 as well). While in the cuspy cases these values are in the same ballpark as in the other models ($\alpha = 0.4 - 1.1$ and $c = 4.4 - 22.9$, in the cases of a flatter core α is negative and large (-2.5 and -5.6) and c is very large ($123 - 238$), meaning that r_c falls outside the range of interest, below $0.01R_V$. This makes the model profile at

very small radii well below $0.01R_v$ irrelevant to what real haloes are likely to look like on such small scales. In fact, in this model the density profile at very small radii is rising with radius and the density vanishes as $r \rightarrow 0$. The main virtue of this model is the excellent match to the variety of halo profiles at $(0.01 - 1)R_v$ with a fully analytic profile and only two free parameters. However, we stress again that for the properties of physical interest one should appeal to quantities such as \bar{s}_1 , \bar{s}_2 and c_m , and one should not extrapolate this profile to radii well outside the range where the fit was performed.

We conclude that the $\bar{\gamma} = 3$ with $\beta = 2$ is an excellent fully analytic profile for fitting the range $(0.01 - 1)R_v$ in haloes of a variety of cusps and cores, given the quality of the fits and having only two free parameters. Its disadvantages for some purposes are the possible large deviations of the profile shape from realistic haloes well outside the range of interest, and the somewhat less simple analytic expressions for the potential and especially for the velocity dispersion compared to the model b1 with $\beta = 1$.

On the other hand, the fit with $\beta = 1$ in Fig. B2, especially in the cases of a core, tends to overestimate the density in the middle halo, near the velocity peak, and to overestimate the inner slope, with $\Delta \sim 0.015 - 0.042$ and $\Delta\bar{s}_1 = 0.16 - 0.42$. As can be seen in §C, the match in the inner slope can be improved by enhanced weighting ($w = 10$) in the inner halo, but this comes at the expense of increasing the deviation in the middle halo. It seems that $\beta = 1$ does not really capture the shapes of the profiles in the middle halo.

With $\beta = 1$, the value of the inner asymptotic slope α is similar to the slope of interest \bar{s}_1 for the cuspy profiles, but α underestimates \bar{s}_1 by $0.2 - 0.3$ for the flatter inner profiles. This implies that for low values of α , in order to evaluate the core profile one should appeal to \bar{s}_1 rather than to α even when $\beta = 1$. The slope of the local $\rho(r)$ at $0.015R_v$ is larger than \bar{s}_1 of $\bar{\rho}(r)$ by the Δs given in eq. (20).

With $\beta = 1$ the values of c are not ridiculously large (as they are for $\beta = 2$). The low values of c compared to model a1 or to the NFW case are due to the need to compensate for the enforced $\bar{\gamma} = 3$ at $r \gg R_v$ (corresponding to $\gamma = 4$ for $\rho(r)$), so the meaning of c is not as straightforward as in these Note that c gets larger in the cored cases, namely c tends to be anti-correlated with α . On the other hand, c_m is somewhat correlated with \bar{s}_1 , so it may serve as an additional characteristic of the cusp-core.

We conclude that the single $\bar{\gamma} = 3$ and $\beta = 1$ model can be used to study the cusp-core when a simple analytic potential is needed, but only if a very accurate fit in the middle halo is not required. We will see in §4.2.5 that the fit becomes excellent overall when a double such model is used. Its advantage is that the analytic expression for the potential is very simple, and the analytic expression for the velocity dispersion is manageable.

4.2.5 Double Profiles with $\bar{\gamma} = 3$, Models c1 and c2

Figure 3 and Fig. B3 refer to the fully analytic double profiles of eq. (34), with $\bar{\gamma} = 3$ and with β either 2 or 1 in models c2 and c1 respectively. The three free parameters are α , c_1 and c_2 . We use fixed weights for the two components, $f_1 = 0.33$ and $f_2 = 0.67$ (giving best fit when fitting $\bar{\rho}$), and uniform weighting ($w = 1$).

With three free parameters, the fits are excellent at all radii in all cases, with $\Delta = 0.005 - 0.015$ dex and $\Delta\bar{s}_1 = 0.03 - 0.17$ for the two values of β . The double profiles capture the inner halo, the peak velocity, and the outskirts. For $\beta = 2$, the quality of fit of the double profile is comparable to that of the single profile, but for $\beta = 1$ the double profile represents a significant improvement over the single profile.

Again, the useful parameter for characterizing the cusp-core is \bar{s}_1 , not α , which is materialized at a smaller radius, not relevant to the core region of interest. The values of α can be negative, especially in the cored haloes, and with $\beta = 2$ they could become very large.

The values of c_1 and c_2 are not straightforward to interpret, and for $\beta = 2$ and cored haloes they become extremely large. The more physical concentration is in a rather narrow range, $c_m = 3.8 - 9.5$, and it has some correlation with \bar{s}_1 , so it can also be used to characterize the cusp-core.

We conclude that the double $\bar{\gamma} = 3$ models are both very well suited for studying the evolution in the cusp-core where an analytic potential is needed, with the $\beta = 1$ double model being a significant improvement over the corresponding single model. For these double models, the quality of fits for $\beta = 2$ and $\beta = 1$ are similar. This argues in favor of preferring the double model with $\beta = 1$ (c1), because the analytic expressions for the potential and velocity dispersion are simpler. However, recall that the single model with $\beta = 2$ (b2) is as accurate, and it involves only two free parameters.

4.2.6 Fits with Enhanced Weighting in the Inner Halo

In §C we present in Table C1 and Figs. C1 to C3 the analogous fits of models to simulated haloes with enhanced weighting of $w = 10$ in the inner halo, $(0.01 - 0.03)R_v$. The fits naturally improve in the cusp-core region for all models and all haloes, with $\Delta\bar{s}_1 = 0.00 - 0.03, 0.01 - 0.10, 0.00 - 0.05$ for models a,b,c respectively. The values of $\Delta\bar{s}_1 = 0.07 - 0.10$ are limited to model b1, but even these represent very small deviations.

The overall fit is somewhat less good than with equal weighting ($w = 1$), with $\Delta = 0.004 - 0.024, 0.009 - 0.083, 0.007 - 0.024$ for models a,b,c respectively. Again, the values of $\Delta = 0.054 - 0.083$ are limited to model b1. In general, the global rms deviations of order 0.01 dex are sensible.

We conclude that when the focus is on the fit in the cusp-core region, one can benefit from applying the fit with enhanced weights at $(0.01 - 0.03)R_v$.

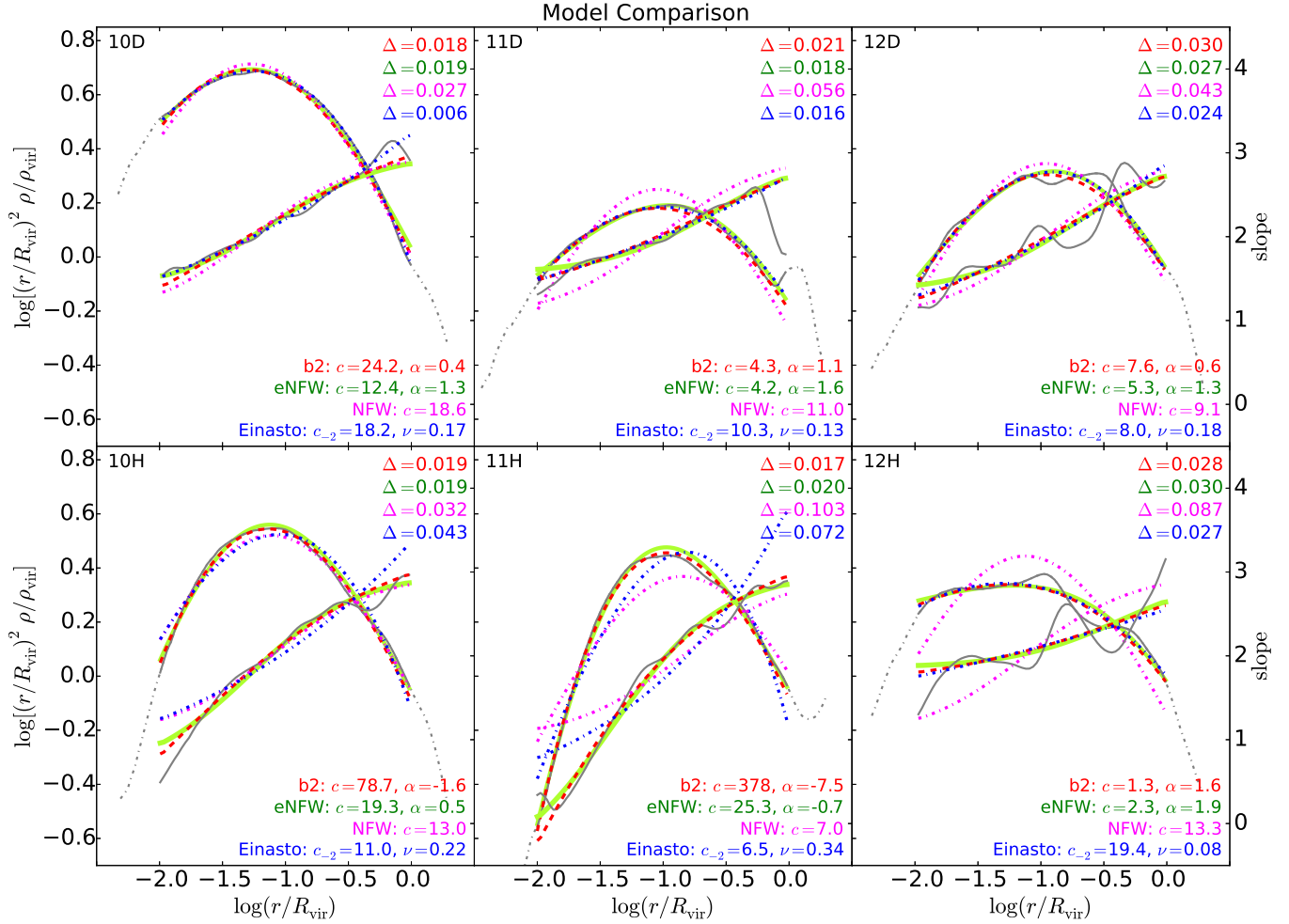


Figure 4. A comparison of models versus the simulated halo profiles, where the best-fit is applied to $\rho(r)$, showing $r^2\rho(r)$ and the slope of $\rho(r)$. Compared are the new analytic profile b2 ($\beta = 2, \tilde{\gamma} = 3$; red), the eNFW profile with α free ($\beta = 1, \gamma = 3$; green), and the Einasto profile (blue), each with two free parameters. Also shown is the one-parameter NFW fit ($\alpha = 1$). The best fits of the analytic b2 model and the eNFW profile are similar, and they are both excellent in quality with low values of Δ for all haloes. The NFW profile is fine for some of the cuspy haloes, but it becomes a poor approximation for other cuspy haloes and for the cored haloes. The Einasto profile does as well as eNFW and the analytic profile in the cuspy cases, but it fails in the cases with a flatter cusp-core, where the density slope profile deviates from a power law.

4.3 Comparison with Popular Non-analytic Models

It would be worthwhile to compare the fits between the new models and other popular models which do not necessarily have analytic expressions for mass-velocity and potential. We compare our model b2 with an extended NFW profile (eNFW) and with the Einasto profile, all having two free parameters.

By eNFW we refer to eq. (1) with $\beta = 1$ and $\gamma = 3$, where α is free in addition to c . We also show for comparison the one-parameter NFW profile where $\alpha = 1$.

The Einasto density profile (Einasto 1965; Navarro et al. 2004) is

$$\rho(r) = \rho_{-2} \exp\left(-\frac{2}{\nu}(x^\nu - 1)\right), \quad x = \frac{r}{r_{-2}}, \quad (37)$$

where r_{-2} is where the slope is -2 and the density is

ρ_{-2} . This is the 3D analog of the Sersic profile used to match the stellar surface density profiles of galaxies. This Einasto density profile has a power-law slope profile,

$$s(r) = -\frac{d \log \rho}{d \log r} = 2 \left(\frac{r}{r_{-2}}\right)^\nu, \quad (38)$$

and the best fit to DMO simulated haloes yields $\nu \simeq 0.17$ (Navarro et al. 2004; Gao et al. 2008; Duffy et al. 2008; Dutton & Macciò 2014).

Figure 4 shows the different best-fit models versus the simulated profiles. Here, we show the profiles of local density $r^2\rho(r)$ and the slope of $\rho(r)$ (rather than the analogous quantities for $\bar{\rho}(r)$ shown in all other figures), because for $\rho(r)$ one has analytic expressions for all models. The fit is performed here on the simulated $\rho(r)$, derived from $M(r)$ via a procedure that involves certain smoothing as described in §4.1.2, with equal weights in log-spaced radii.

The best fits of the analytic b2 model and the eNFW profile are rather similar, and they are both excellent in quality for all haloes, with $\Delta = 0.018 - 0.030$. In the cuspy cases, the Einasto profile does as well and even slightly better than the eNFW and analytic profiles, with $\Delta = 0.006 - 0.027$, but it fails in the cases with a flatter cusp-core, where the density slope profile deviates from a power law, with $\Delta = 0.043 - 0.072$. The NFW profile is fine for some of the cuspy haloes, though not as good as the two-parameter profiles. NFW is a poor approximation for other cuspy haloes, and for the cored haloes, with $\Delta = 0.032 - 0.103$.

We conclude that the matches of our new two-parameter profile to the simulated profiles are similar in quality to other existing profiles with a similar number of free parameters. The virtue of the new profile is the analytic expressions for the mass-velocity, potential, and velocity dispersion. The analytic models with three parameters provide slightly better fits, comparable to other profiles with three free parameters, with the advantage of analytic mass-velocity profiles.

5 CONCLUSION

Our proposed functional form for the *mean* density profile of spherical DM haloes, with a varying asymptotic inner slope α , is based on eq. (3). By expressing the mean density (rather than the local density) in simple analytic terms, the mass, velocity and force profiles are automatically expressed analytically, and the local density profile is easily derived. The most flexible functional form involves four parameters, α , β , $\bar{\gamma}$ and c . In principle, β and $\bar{\gamma}$ can vary, but in practice $\beta \simeq 2$ yields excellent fits, and $\beta = 1$ can also provide good fits in certain models.

When the asymptotic outer slope of $\bar{\rho}(r)$ is fixed at $\bar{\gamma} = 3$, and β is a natural number such that the asymptotic slope of $\rho(r)$ is $\gamma = \bar{\gamma} + \beta^{-1}$, there are also *analytic* expressions for the *potential* and velocity dispersion. These provide a new useful tool for theoretical studies of halo evolution and for constructing model haloes. With the introduction of a free concentration parameter c , the $\bar{\gamma} = 3$ profiles have the flexibility for matching the outer slopes of DM-halo profiles.

The six models tested here, all with either $\beta = 2$ or $\beta = 1$, are (a) a flexible model with three free parameters α , c and $\bar{\gamma}$, (b) a model with $\bar{\gamma} = 3$ and two free parameters α and c , and (c) a double profile, a sum of models as in b, with three free parameters α , c_1 and c_2 . Models a have *analytic mass and velocity profiles*. Models b and c have in addition *analytic expressions for the potential and velocity-dispersion profiles*.

We evaluate the relative quality of these models by performing fits to profiles of six DM haloes from cosmological simulations without and with baryons, in which the inner profiles range from a steep cusp to a flat core.

We find that the best fits are provided by models a2, b2, and c1 or c2. This says that in general $\beta = 2$ captures better the shape of the profile in the middle

halo, but a double profile with $\beta = 1$ can mimic a similar shape in the middle halo.

If an excellent fit is desired at all radii, with analytic mass-velocity profiles but without a need for an analytic potential, and if the fit has to extend well beyond the virial radius, the flexible model a2 with a free $\bar{\gamma}$ is a good choice. If an even better accuracy is desired, this model can be applied with a free β .

If an *analytic potential* is required, the minimal model b2, with $\beta = 2$ and only two free parameters, is our best choice. The encouraging finding is that model b2 provides fits almost as good as the three-parameter models. Therefore, there is no much gain in extending it to the double model c2.

Model b1 has somewhat simpler expressions for the potential and velocity dispersion, but its fits to the simulated haloes are somewhat less accurate. It is therefore the choice when the accuracy of the fits is not a major issue. However, if an excellent fit is desired, as well as simple analytic expressions, the choice is the double model c1, with $\beta = 1$.

We find that our analytic two-parameter model b2 matches the simulated profiles as well as the popular eNFW and Einasto profiles, which have the same number of parameters but no analytic expressions for mass-velocity and potential. In fact, model b2 does much better than Einasto in the case of cored haloes. Our analytic double models do as well as other non-analytic three-parameter models.

The free parameters in the functional form, the asymptotic slopes α and $\bar{\gamma}$ and the concentration parameter(s), are not always useful for directly interpreting the shape of the profile in the range of interest, $(0.01 - 1)R_v$. This is true in particular for the models with $\beta = 2$, where the profile well outside this radius range can be a very poor fit to the actual halo profiles. A general warning is that an extrapolation of a best-fit model to outside the fitting range is risky, and may be totally unrealistic, e.g., when $\beta = 2$.

The profile is characterized better by more physical parameters that can be derived from the free parameters of the functional form. The physical parameters are, for example, the actual slopes of $\bar{\rho}(r)$ in the regions of interest, e.g., \bar{s}_1 and \bar{s}_2 , and the alternative concentration parameter c_m , which refers to the radius where the slope of $\bar{\rho}(r)$ is -2 and where the velocity curve peaks.

We reiterate that the main purpose of this paper is to provide a new tool for studying the evolution of dark-matter halo profiles, where there are fully *analytic* expressions for the mass and velocity profiles and in particular for the gravitational *potential* and velocity dispersion profiles. For example, model b2, with $\bar{\gamma} = 3$ and $\beta = 2$, is being successfully used in an analytic study of the evolution of the inner halo profiles due to episodes of gas inflow and rapid outflow (Dekel et al, 2017, in prep.).

ACKNOWLEDGMENTS

We acknowledge stimulating discussions with Andi Burkert and Frank van den Bosch. This work was partly supported by the grants ISF 124/12, I-CORE Program of the PBC/ISF 1829/12, BSF 2014-273, PICS 2015-18, GIF I-1341-303.7/2016, and NSF AST-1405962. The simulations were performed on the THEO cluster of the Max-Planck-Institut für Astronomie and the HYDRA cluster at the Rechenzentrum in Garching; and the Milky Way supercomputer, funded by the Deutsche Forschungsgemeinschaft (DFG) through Collaborative Research Center (SFB 881) “The Milky Way System” (subproject Z2), hosted and co-funded by the Jülich Supercomputing Center (JSC).

REFERENCES

- Ade P. A. R., Aghanim N., Arnaud M., Ashdown M., Aumont J., Baccigalupi C., et al., 2014, *A&A*, 561, A97
- Burkert A., 1995, *ApJ*, 447, L25
- Chabrier G., 2003, *PASP*, 115, 763
- de Blok W. J. G., McGaugh S. S., Bosma A., Rubin V. C., 2001, *ApJ*, 552, L23
- Dehnen W., 1993, *MNRAS*, 265, 250
- Di Cintio A., Brook C. B., Dutton A. A., Macciò A. V., Stinson G. S., Knebe A., 2014, *MNRAS*, 441, 2986
- Diemer B., Kravtsov A. V., 2014, *ApJ*, 789, 1
- Duffy A. R., Schaye J., Kay S. T., Dalla Vecchia C., 2008, *MNRAS*, 390, L64
- Dutton A. A., Macciò A. V., 2014, *MNRAS*, 441, 3359
- Dutton A. A. et al., 2016a, *MNRAS*, 461, 2658
- Dutton A. A., Macciò A. V., Frings J., Wang L., Stinson G. S., Penzo C., Kang X., 2016b, *MNRAS*, 457, L74
- Einasto J., 1965, *Trudy Astrofizicheskogo Instituta Alma-Ata*, 5, 87
- Evans N. W., 1994, *MNRAS*, 267, 333
- Gao L., Navarro J. F., Cole S., Frenk C. S., White S. D. M., Springel V., Jenkins A., Neto A. F., 2008, *MNRAS*, 387, 536
- Gill S. P. D., Knebe A., Gibson B. K., 2004, *MNRAS*, 351, 399
- Goerdt T., Moore B., Read J. I., Stadel J., Zemp M., 2006, *MNRAS*, 368, 1073
- Graham A. W., Merritt D., Moore B., Diemand J., Terzić B., 2006, *AJ*, 132, 2701
- Gutcke T. A., Stinson G. S., Macciò A. V., Wang L., Dutton A. A., 2017, *MNRAS*, 464, 2796
- Hernquist L., 1990, *ApJ*, 356, 359
- Jaffe W., 1983, *MNRAS*, 202, 995
- Jing Y. P., Suto Y., 2000, *ApJ*, 529, L69
- Keller B. W., Wadsley J., Benincasa S. M., Couchman H. M. P., 2014, *MNRAS*, 442, 3013
- Knollmann S. R., Knebe A., 2009, *ApJS*, 182, 608
- Levenberg K., 1944, *Quarterly of Applied Mathematics*, 2, 164
- Marquardt D., 1963, *SIAM Journal of Applied Mathematics*, 11, 431
- Merritt D., Graham A. W., Moore B., Diemand J., Terzić B., 2006, *AJ*, 132, 2685
- More S., Diemer B., Kravtsov A. V., 2015, *ApJ*, 810, 36
- Navarro J. F., Frenk C. S., White S. D. M., 1997, *ApJ*, 490, 493
- Navarro J. F. et al., 2004, *MNRAS*, 349, 1039
- Obreja A., Stinson G. S., Dutton A. A., Macciò A. V., Wang L., Kang X., 2016, *MNRAS*, 459, 467
- Oh S.-H., Brook C., Governato F., Brinks E., Mayer L., de Blok W. J. G., Brooks A., Walter F., 2011, *AJ*, 142, 24
- Oldham L. J., Auger M. W., 2016, *MNRAS*, 457, 421
- Savitzky A., Golay M. J. E., 1964, *Analytical Chemistry*, 36, 1627
- Schaller M. et al., 2015, *MNRAS*, 451, 1247
- Shen S., Wadsley J., Stinson G., 2010, *MNRAS*, 407, 1581
- Stinson G., Seth A., Katz N., Wadsley J., Governato F., Quinn T., 2006, *MNRAS*, 373, 1074
- Stoehr F., 2006, *MNRAS*, 365, 147
- Swaters R. A., Madore B. F., van den Bosch F. C., Balcells M., 2003, *ApJ*, 583, 732
- Tollet E. et al., 2016, *MNRAS*, 456, 3542
- Tremaine S., Richstone D. O., Byun Y.-I., Dressler A., Faber S. M., Grillmair C., Kormendy J., Lauer T. R., 1994, *AJ*, 107, 634
- Wadsley J. W., Stadel J., Quinn T., 2004, *Nature*, 9, 137
- Walker M. G., Peñarrubia J., 2011, *ApJ*, 742, 20
- Wang L., Dutton A. A., Stinson G. S., Macciò A. V., Gutcke T., Kang X., 2017, *MNRAS*
- Wang L., Dutton A. A., Stinson G. S., Macciò A. V., Penzo C., Kang X., Keller B. W., Wadsley J., 2015, *MNRAS*, 454, 83
- Zhao H., 1996, *MNRAS*, 278, 488

APPENDIX A: GENERAL ANALYTIC PROFILES

This appendix summarizes the results from Zhao (1996) for the family of local density profiles

$$\rho(x) \propto \frac{1}{x^\alpha (1 + x^{1/n})^{n(3+k/n-\alpha)}}, \quad (\text{A1})$$

where n and k are natural numbers.⁶ Defining

$$\chi(x) = \frac{x^{1/n}}{1 + x^{1/n}}, \quad (\text{A2})$$

the density becomes

$$\rho(x) \propto \chi^{-n\alpha} (1 - \chi)^{3n+k}. \quad (\text{A3})$$

The mass profile is

$$M(r) \propto \sum_{i=0}^{k-1} a_i \chi^{n(3-\alpha)+i}, \quad (\text{A4})$$

where

$$a_i = \frac{n}{n(3-\alpha)+i} q(k-1, i), \quad (\text{A5})$$

⁶ We denote by α what Zhao (1996) denote as γ .

and

$$q(i, j) = (-1)^j \frac{i!}{j!(1-j)!}, \quad i \geq j \geq 0 \quad (\text{A6})$$

$$= 0, \quad \text{otherwise.}$$

To be consistent with our notation, one should normalize the mass and density profiles to obtain $M(R_v) = M_v$.

Assuming here that the halo density profile extends to infinity (while we assume that it is truncated at R_t), and that the potential vanishes at infinity, the potential is

$$U(r) \propto - \sum_{i=0}^{n+k-2} b_i S_{n(2-\alpha)+1}(\chi), \quad (\text{A7})$$

where

$$b_i = n \sum_{j=0}^i q(n-1, j) a_{i-j}, \quad (\text{A8})$$

and

$$S_i(\chi) = \frac{1 - \chi^i}{i}, \quad i \neq 0 \quad (\text{A9})$$

$$= -\log \chi, \quad i = 0.$$

The velocity dispersion is

$$\sigma^2(r) \propto \frac{1}{\rho(r)} \sum_{i=0}^{4n+2k-2} d_i S_{2n(1-\alpha)+i}(\chi), \quad (\text{A10})$$

where

$$d_i = \sum_{j=0}^i e_i a_{i-j}, \quad (\text{A11})$$

and

$$e_i = nq(4n+k-1, i). \quad (\text{A12})$$

APPENDIX B: FIT TO SIMULATIONS WITH $\beta = 1$

In §4.2 we present and discuss the fits of our new models to simulations. Table 1 summarizes the results of these fits, and Figs. 1 to 3 help visualize the fits for the models with $\beta = 2$ (models a2, b2 and c2). Here we complement this visual presentation in Figs. B1 to B3 which show the fits for the analogous models with $\beta = 1$ (models a1, b1 and c1). These fits are discussed in §4.2.

APPENDIX C: FIT TO SIMULATIONS WITH ENHANCED WEIGHTING IN THE INNER HALO

To complement the fits to simulations described in §4.2 with uniform weighting at equally spaced log radii in the range $(0.01 - 1)R_v$, we show here analogous fits with enhanced weight, $w = 10$, in the cusp-core region $(0.01 - 0.03)R_v$. The results for $w = 10$ are summarized in Table C1, to be compared to Table 1 for uniform weighting. Figures C1 to (C3) refer to models a2, b2, and c2, the same functional forms as in Figs. 1 to (3), all with $\beta = 2$, but here with enhanced weighting in the inner halo.

. With the enhanced weighting in the inner halo, the fits in the cusp-core regions are naturally slightly better, as measured for example by $\Delta \bar{s}_1$. This comes at the expense of the overall quality of the fits, as expressed for example by Δ .

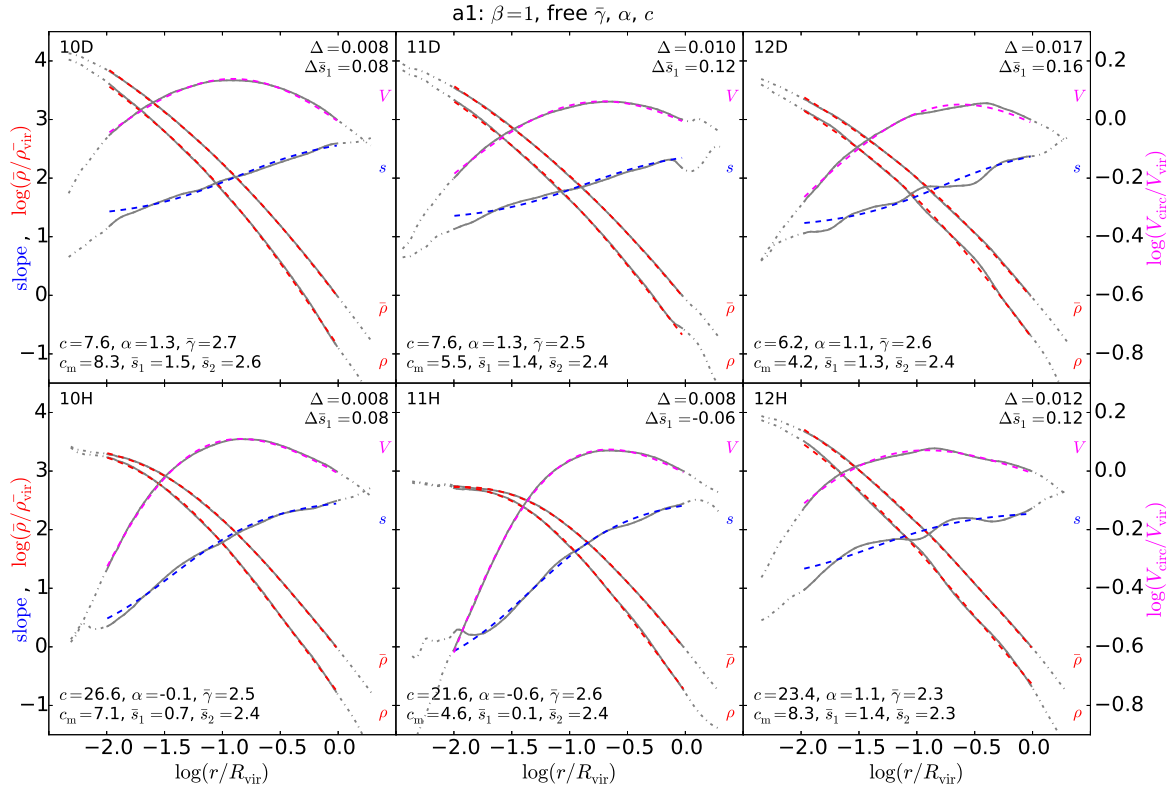


Figure B1. Same as Fig. 1, for the flexible model, but for $\beta = 1$ (model a1). The fits are excellent, with $\Delta = 0.008 - 0.017$ and $\Delta \bar{s}_1 = 0.06 - 0.16$, but not as good as the fits with $\beta = 2$.

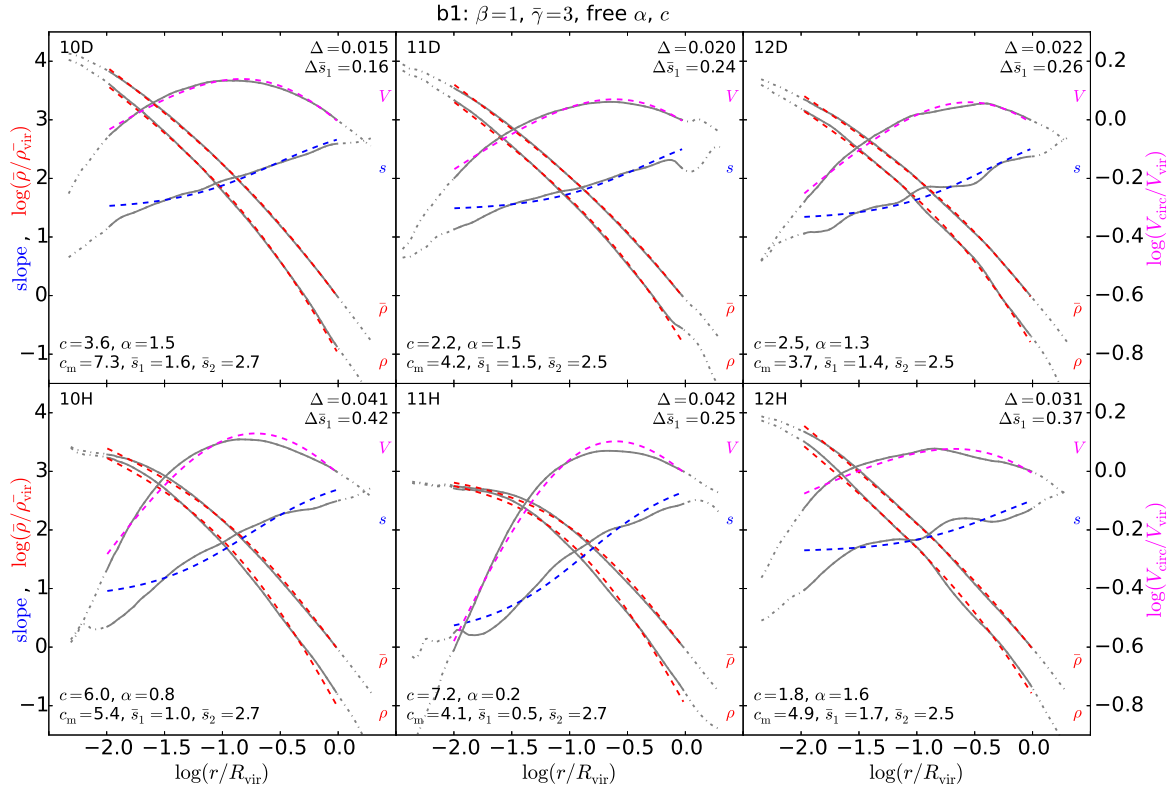


Figure B2. Same as Fig. 2, for the two-parameter analytic model, but for $\beta = 1$ (model b1). The fits are fine in the cuspy haloes, with $\Delta = 0.015 - 0.031$ and $\Delta \bar{s}_1 = 0.16 - 0.37$, but less so in the middle halo in the cored cases, with $\Delta = 0.041 - 0.042$ and $\Delta \bar{s}_1 = 0.25 - 0.42$. The $\beta = 2$ model (b2) is significantly better.

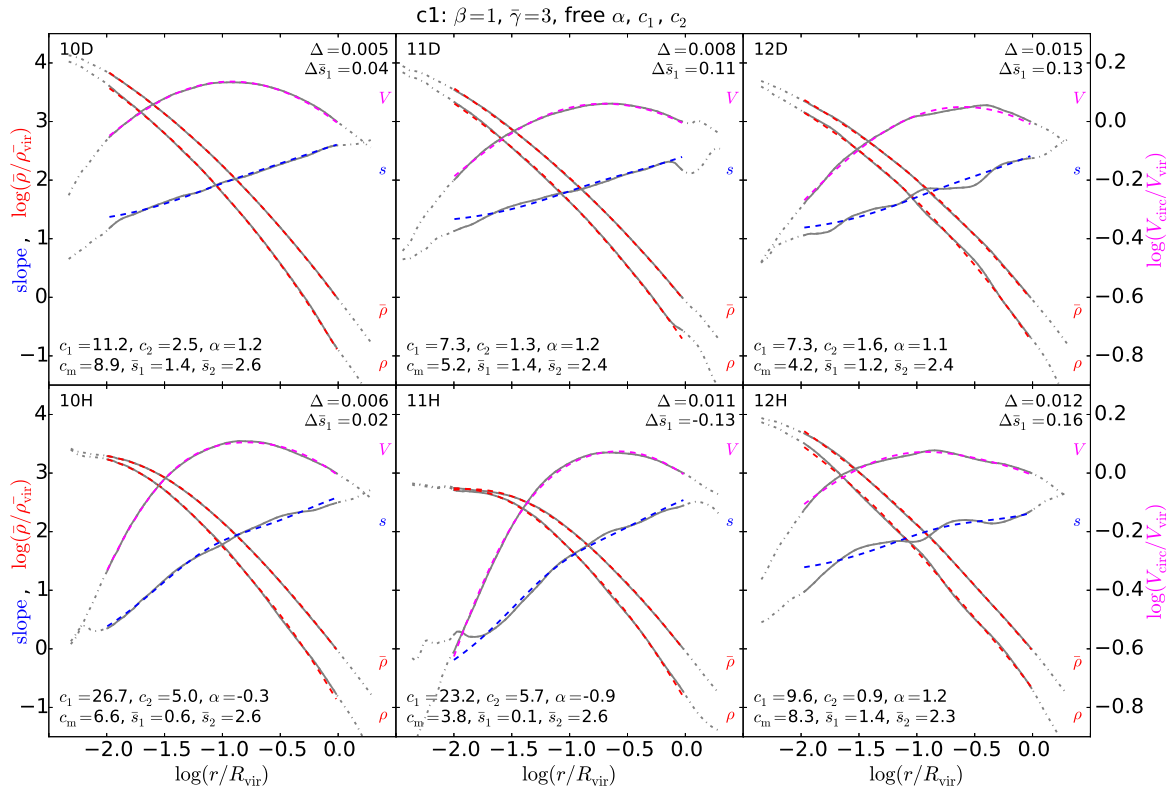


Figure B3. Same as Fig. 3, for the double analytic model, but for $\beta = 1$ (model c1). The fits are excellent, with $\Delta = 0.005 - 0.015$ and $\Delta \bar{s}_1 = 0.02 - 0.16$, comparable to the fits of model c2 where $\beta = 2$.

halo #		1	2	3	4	5	6							
name		10D	11D	12H	12D	10H	11H							
\bar{s}_1		1.4	1.3	1.3	1.1	0.6	0.2							
#	model	params												
a1	$\bar{\gamma}$ free, $\beta = 1$	Δ $\Delta\bar{s}_1$	0.012	0.00	0.017	0.01	0.020	-0.02	0.024	0.01	0.012	0.01	0.013	-0.02
		c c_m	12.7	9.5	18.9	6.4	99.6	10.8	16.0	5.1	36.4	7.5	17.6	4.6
		α \bar{s}_1	1.2	1.4	1.0	1.3	-0.1	1.3	0.8	1.1	-0.4	0.6	-0.5	0.2
		$\bar{\gamma}$ \bar{s}_2	2.6	2.5	2.3	2.3	2.2	2.2	2.4	2.3	2.5	2.4	2.6	2.5
a2	$\bar{\gamma}$ free, $\beta = 2$	Δ $\Delta\bar{s}_1$	0.007	-0.01	0.012	0.01	0.012	0.00	0.018	0.01	0.004	0.00	0.023	-0.03
		c c_m	13.6	8.9	43.8	5.9	1.7e5	8.9	26.2	4.5	468	6.6	32.3	4.1
		α \bar{s}_1	0.6	1.4	0.2	1.3	-56.4	1.3	0.1	1.1	-5.4	0.6	-2.1	0.2
		$\bar{\gamma}$ \bar{s}_2	3.1	2.6	2.7	2.3	2.4	2.3	2.8	2.3	2.9	2.5	3.4	2.6
b1	$\bar{\gamma} = 3$, $\beta = 1$	Δ $\Delta\bar{s}_1$	0.035	0.03	0.054	0.07	0.083	0.10	0.056	0.07	0.079	0.08	0.062	0.01
		c c_m	5.1	7.8	3.7	5.2	4.2	6.0	4.0	4.5	10.7	6.6	9.9	4.6
		α \bar{s}_1	1.3	1.4	1.2	1.3	1.3	1.4	1.1	1.2	0.3	0.7	-0.2	0.2
		\bar{s}_2		2.7		2.6		2.7		2.6		2.8		2.7
b2	$\bar{\gamma} = 3$, $\beta = 2$	Δ $\Delta\bar{s}_1$	0.009	-0.01	0.017	0.03	0.046	0.05	0.020	0.02	0.015	0.01	0.024	-0.05
		c c_m	20.6	9.5	9.6	5.5	14.2	7.3	12.3	4.5	185	6.6	134	4.1
		α \bar{s}_1	0.5	1.4	0.6	1.3	0.6	1.3	0.3	1.1	-3.4	0.6	-3.9	0.2
		\bar{s}_2		2.5		2.4		2.5		2.4		2.6		2.5
c1	x2 $\bar{\gamma} = 3$, $\beta = 1$	Δ $\Delta\bar{s}_1$	0.007	0.00	0.015	0.02	0.022	0.02	0.021	0.02	0.007	0.00	0.018	-0.03
		c_1 c_m	13.3	9.5	10.1	6.4	14.3	10.8	10.3	4.8	27.7	6.6	19.3	4.1
		c_2 \bar{s}_1	2.5	1.4	1.3	1.3	1.0	1.3	1.6	1.1	5.0	0.6	6.0	0.2
		α \bar{s}_2	1.1	2.6	1.1	2.4	1.0	2.3	0.9	2.4	-0.4	2.6	-0.6	2.6
c2	x2 $\bar{\gamma} = 3$, $\beta = 2$	Δ $\Delta\bar{s}_1$	0.009	-0.01	0.009	0.01	0.011	-0.02	0.016	0.00	0.011	0.01	0.024	-0.05
		c_1 c_m	20.6	9.5	74.1	5.2	761	7.8	58.9	4.2	3.0e3	6.6	134	4.1
		c_2 \bar{s}_1	20.6	1.4	11.3	1.3	64.6	1.3	13.3	1.1	1.1e3	0.6	134	0.2
		α \bar{s}_2	0.5	2.5	-0.4	2.4	-4.5	2.4	-0.5	2.4	-14.1	2.6	-3.9	2.5

Table C1. Same as Table 1, but with enhanced weighting of $w = 10$ in the inner halo, $(0.01 - 0.03)R_v$. The fits are naturally better in the cusp-core region, at the expense of the global fit, which is slightly less good.

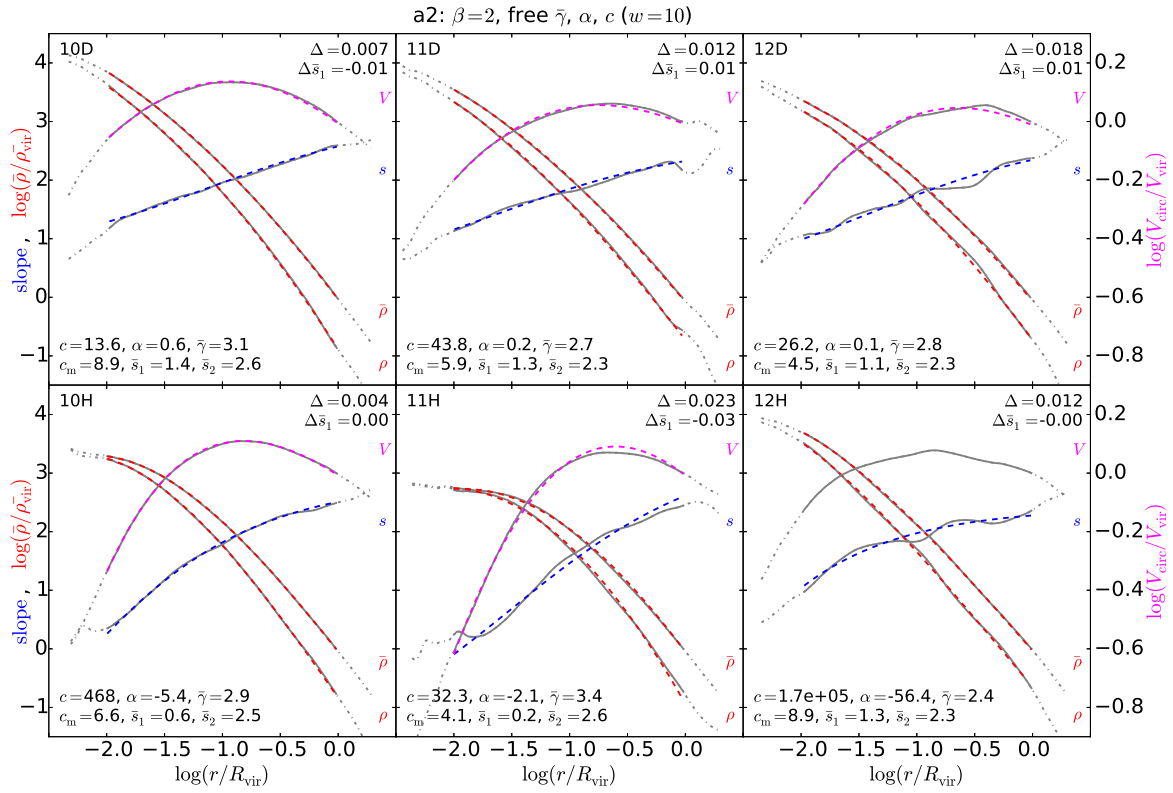


Figure C1. Same as Fig. 1, for the flexible model with $\beta = 2$ (model a2), but with enhanced weighting $w = 10$ in the fit at $(0.01-0.03)R_v$. The fits in the inner halo are excellent, with $\Delta\bar{s}_1 = 0.00 - 0.03$. The overall fit is also good, $\Delta = 0.004 - 0.023$, though less good than with uniform weighting, especially in the cored halo 11H.

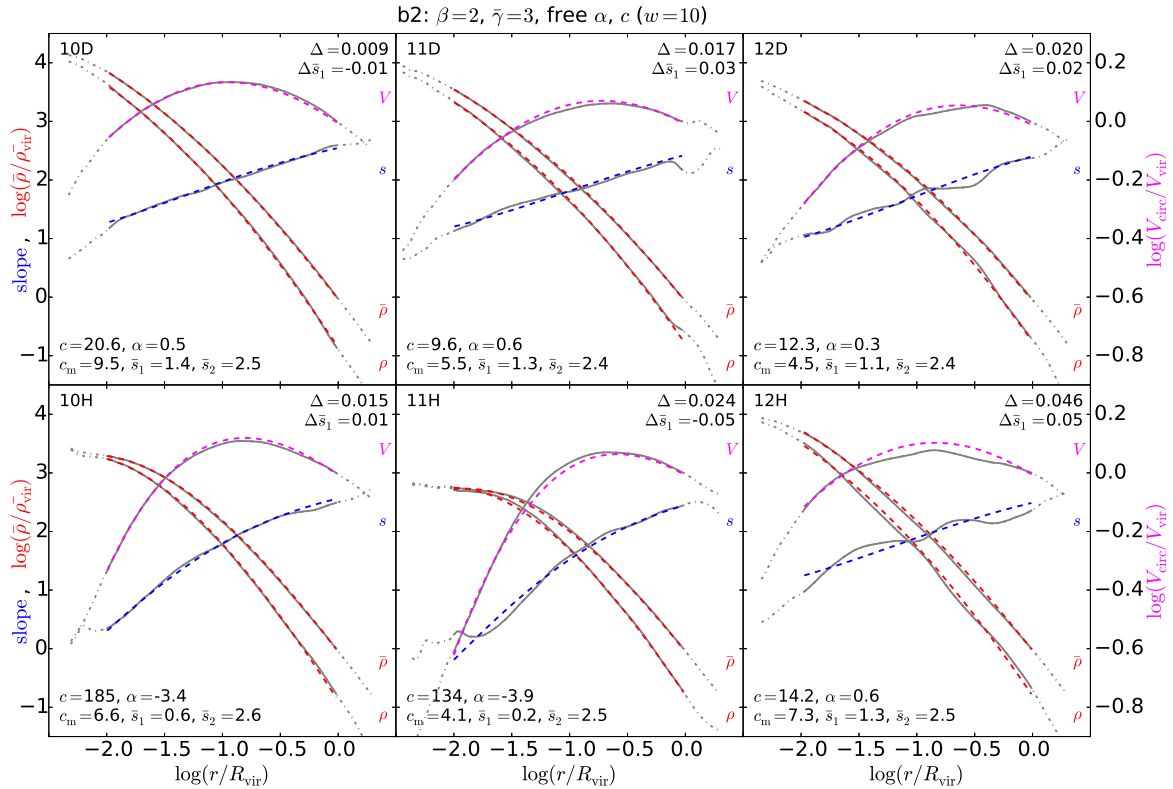


Figure C2. Same as Fig. 2, for the two-parameter analytic model with $\beta = 2$ (model b2), but with enhanced weighting $w = 10$ in the fit at $(0.01-0.03)R_v$. The fits in the inner halo are excellent, with $\Delta\bar{s}_1 = 0.01 - 0.05$. The overall fit is also fine, $\Delta = 0.009 - 0.046$, though less good than with uniform weighting, especially in the very cuspy halo 12H.

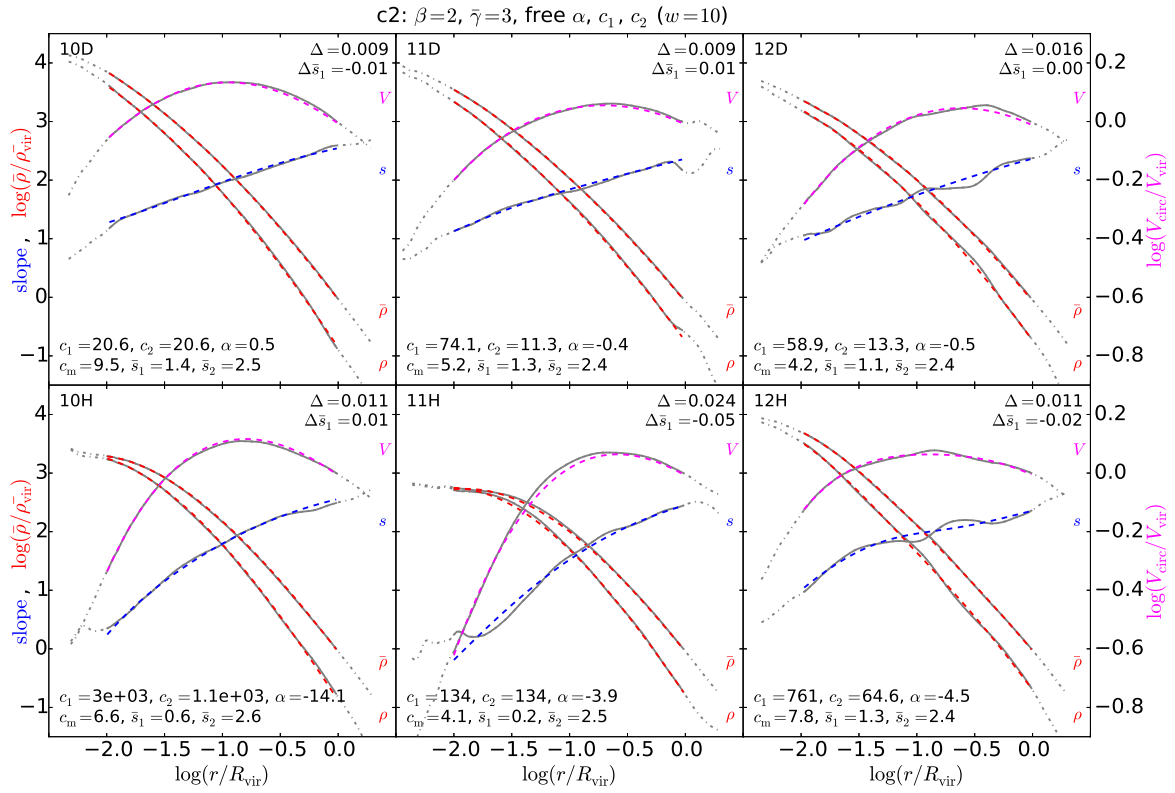


Figure C3. Same as Fig. 3, for the double analytic model with $\beta = 2$ (model c2), but with enhanced weighting $w = 10$ in the fit at $(0.01 - 0.03)R_v$. The fits in the inner halo are excellent, with $\Delta \bar{s}_1 = 0.00 - 0.05$. The overall fit is also good, with $\Delta = 0.009 - 0.024$, though less good than with uniform weighting.